PB89-189625

# SMALL-SCALE MODELING TECHNIQUES FOR REINFORCED CONCRETE STRUCTURES SUBJECTED TO SEISMIC LOADS

by

W. Kim, A. El-Attar and R. N. White

Department of Structural Engineering
School of Civil and Environmental Engineering
Cornell University
Ithaca, New York 14853

Technical Report NCEER-88-0041

November 22, 1988

# NOTICE

This report was prepared by Cornell University as a result of research sponsored by the National Center for Earthquake Engineering Research (NCEER). Neither NCEER, associates of NCEER, its sponsors, Cornell University or any person acting on their behalf:

a. makes any warranty, express or implied, with respect to the use of any information, apparatus, method, or process disclosed in this report or that such use may not infringe upon privately owned rights; or

b. assumes any liabilities of whatsoever kind with respect to the use of, or the damage resulting from the use of, any information, apparatus, method or process disclosed in this report.

# SMALL-SCALE MODELING TECHNIQUES FOR REINFORCED CONCRETE STRUCTURES SUBJECTED TO SEISMIC LOADS

by

Woo Kim[1], Adel El-Attar[2] and Richard N. White[3]

November 22, 1988

Technical Report NCEER-88-0041

1  Post-doctoral Associate, Department of Structural Engineering, School of Civil and Environmental Engineering, Cornell University
2  Graduate Student, Department of Structural Engineering, School of Civil and Environmental Engineering, Cornell University
3  James A. Friend Family Professor of Engineering, School of Civil and Environmental Engineering, Cornell University

NATIONAL CENTER FOR EARTHQUAKE ENGINEERING RESEARCH
State University of New York at Buffalo
Red Jacket Quadrangle, Buffalo, NY 14261

# PREFACE

The National Center for Earthquake Engineering Research (NCEER) is devoted to the expansion and dissemination of knowledge about earthquakes, the improvement of earthquake-resistant design, and the implementation of seismic hazard mitigation procedures to minimize loss of lives and property. The emphasis is on structures and lifelines that are found in zones of moderate to high seismicity throughout the United States.

NCEER's research is being carried out in an integrated and coordinated manner following a structured program. The current research program comprises four main areas:

- Existing and New Structures
- Secondary and Protective Systems
- Lifeline Systems
- Disaster Research and Planning

This technical report pertains to Program 1, Existing and New Structures, and more specifically to system response investigations.

The long term goal of research in Existing and New Structures is to develop seismic hazard mitigation procedures through rational probabilistic risk assessment for damage or collapse of structures, mainly existing buildings, in regions of moderate to high seismicity. The work relies on improved definitions of seismicity and site response, experimental and analytical evaluations of systems response, and more accurate assessment of risk factors. This technology will be incorporated in expert systems tools and improved code formats for existing and new structures. Methods of retrofit will also be developed. When this work is completed, it should be possible to characterize and quantify societal impact of seismic risk in various geographical regions and large municipalities. Toward this goal, the program has been divided into five components, as shown in the figure below:

**Program Elements:**

Seismicity, Ground Motions and Seismic Hazards Estimates

Geotechnical Studies, Soils and Soil-Structure Interaction

System Response: Testing and Analysis

Reliability Analysis and Risk Assessment

Expert Systems

**Tasks:**

Earthquake Hazards Estimates,
Ground Motion Estimates,
New Ground Motion Instrumentation,
Earthquake & Ground Motion Data Base.

Site Response Estimates,
Large Ground Deformation Estimates,
Soil-Structure Interaction.

Typical Structures and Critical Structural Components:
Testing and Analysis;
Modern Analytical Tools.

Vulnerability Analysis,
Reliability Analysis,
Risk Assessment,
Code Upgrading.

Architectural and Structural Design,
Evaluation of Existing Buildings.

System response investigations constitute one of the important areas of research in Existing and New Structures. Current research activities include the following:

1. Testing and analysis of lightly reinforced concrete structures, and other structural components common in the eastern United States such as semi-rigid connections and flexible diaphragms.
2. Development of modern, dynamic analysis tools.
3. Investigation of innovative computing techniques that include the use of interactive computer graphics, advanced engineering workstations and supercomputing.

The ultimate goal of projects in this area is to provide an estimate of the seismic hazard of existing buildings which were not designed for earthquakes and to provide information on typical weak structural systems, such as lightly reinforced concrete elements and steel frames with semi-rigid connections. An additional goal of these projects is the development of modern analytical tools for the nonlinear dynamic analysis of complex structures.

*As part of NCEER's program in existing structures, researchers are investigating the response characteristics of various building materials under earthquake conditions. In this study, researchers have focused attention on improving the materials used to construct small-scale reinforced concrete structures. As a result, a model was developed and its behavior compared to a prototype structure to determine which provides the best modeling of cracking and hysteretic behavior. The results from the study provide new information on model materials, which will be of immediate use to engineers contemplating small-scale modeling of reinforced concrete structures.*

**ABSTRACT**

This report focuses on improved physical modeling techniques for small-scale reinforced concrete structures subjected to seismic loadings. Particular emphasis is placed on the development of a model concrete mix to accurately model the important strength and stiffness properties of full-scale prototype concrete. The gradation of aggregate used in the mix, along with the aggregate to cement ratio, are shown to be critical in achieving sufficiently low tensile strength while still maintaining acceptable critical strain levels at compressive failure of the model concrete. Four types of model reinforcement with different bond characteristics are also studied, including determination of appropriate heat treatment processes to achieve accurate values of yield point and acceptable post-yield characteristics. This new information on model materials will be of immediate use to engineers contemplating small scale modeling of reinforced concrete structures.

Using these model materials, the adequacy of bond between model concrete and model reinforcement is then examined with experiments on a series of 1/6 scale model assemblages of a prototype beam subjected to reversing loads. The cantilever beam section (prototype and model) are loaded in fully reversing bending at gradually increasing ductility levels up to a maximum value of 6. The resulting load-deflection hysteresis loops are compared (model to prototype) and it is concluded that small scale elements fabricated with annealed, *threaded rod* reinforcement best meet the similitude requirements for strength, stiffness, and (in particular), cyclic degradation of stiffness, energy absorption during fully reversing loads, and failure mode after severe cycling.

# TABLE OF CONTENTS

LIST OF FIGURES

## LIST OF FIGURES (Continued)

## LIST OF TABLES

# SECTION 1

## INTRODUCTION

### 1.1 Statement of the Problem

The study of dynamic structural response of full scale reinforced concrete structures subjected to earthquake loadings requires testing facilities with extremely high load capacities, and is possible at only a few highly-specialized laboratories. The cost of using these facilities, and of building and disposing of the test specimens, is very high. For this reason, small-scale structural models (at geometric scale factors in the range of 1/6 to 1/10) offer an attractive means to perform dynamic loading experiments without incurring the high costs of full-scale testing. The major problem met in small-scale modeling of reinforced concrete structures is meeting similitude requirements sufficiently well to capture the many subtle behavioral modes as the structure is loaded to failure.

When a prototype reinforced concrete system is modeled for strength, it is necessary to reproduce all significant physical characteristics on a one-one basis. Any distortion of similitude must be understood and its effects must be predictable. These distortions, which result in the so-called "scale effects," must be minimized through application of the very best modeling techniques and practices. The model concrete mix should be proportioned to match the compressive stress-strain characteristics of the prototype concrete while minimizing the overly high tensile strengths so often found in model concretes. Model reinforcement should have a stress-strain curve identical to that of the prototype reinforcement, including the strain-hardening region. Furthermore, bond behavior, which is the single most important measure of the composite action between the concrete and reinforcement, should be similar (if not identical) in prototype and model.

Although considerable improvement in model materials has been realized in the past three decades [3], there are limitations (mainly materials-driven) on the use of small-scale models. This study was conducted to develop improved model materials and modeling techniques for reinforced concrete structures, particularly for seismic-type loading histories.

## 1.2 Organization of the Study

The first part of this study (Section 2) was aimed at obtaining the model concrete that best achieved the desired similitude conditions on strength, ultimate strain capacities, and stiffness. This was done by developing a series of new mixes and comparing their properties with those of a typical 4500 psi design strength prototype concrete.

Section 3 of the report deals with model reinforcement, including selection of the most appropriate type of small deformed bars, and details on the heat treatment processes used to achieve the desired properties.

In Section 4 the model materials are used in a testing program designed to simulate the severe demands placed on reinforced concrete elements in a structure subjected to seismic loading. A prototype structure was built and tested to failure under a series of fully reversing cyclic loads of gradually increasing intensity. One-sixth scale models of the same design were then tested using several different types of model reinforcement, and the results of the models were compared with that of the prototype.

The report concludes with a summary of results and conclusions in Section 5. Specific recommendations are made on the best choices for model concrete and model reinforcement for building reinforced concrete models with beam and column cross-sectional dimensions on the order of 1 to 2 inches.

# SECTION 2
## MODEL CONCRETE

### 2.1 Introduction

One of the most difficult steps in small scale modeling is the selection of model concrete. Accurate duplication of the prototype concrete properties is required if the model is to simulate the whole range of behavior of the structural system as it is loaded to failure. It is generally required that a model concrete have specific values of four properties under short-term load:

1. Ultimate compressive strength, $f_c'$

2. Tangent or secant modulus of elasticity, $E$

3. Ultimate compressive strain $e_u$

4. Ultimate tensile strength, $f_t'$

Various studies using microconcrete (defined here as concrete made from Portland cement, water, and sand without coarse aggregate) have shown that reasonably adequate results can be obtained if the material is controlled properly (references [2,3,4]). Thus, microconcrete is the logical choice as a concrete substitute in small scale models. Other cementitious materials such as gypsum have also been used in model concretes with reasonable success.

However, it is acknowledged in the literature that microconcrete usually has lower stiffness, larger compressive strain capacity, and higher tensile strength than regular prototype concrete with the same compressive strength [5]. The lower stiffness and larger compressive strain capacity result in distortion of strains in the model, which may or may not be important, depending upon the particular failure mode in the model structure. The higher tensile strength has many implications for model response -- delayed tensile cracking, improved bond performance, higher diagonal tension (shear) capacity, and less damage and degradation under cyclic loadings. Hence the study reported here was undertaken to obtain a better microconcrete which could be considered fully adequate for the purpose of modeling dynamic repsonse of reinforced concrete structures.

Properties of a typical prototype concrete with a design strength of 4500 psi were established first. This was followed by development and testing of a variety of microconcrete mixes.

## 2.2  Test Program

### 2.2.1  Materials

The properties of a heterogenous material, such as concrete, cannot be easily simulated because of the inherent complexity of the many factors that influence the properties of the hardened (cured) concrete. Theoretically, the scaling of concrete properties requires not only appropriate scaling of aggregate size, but also scaling of pore size in the gel and of void size in the hardened mixture. Although some of these requirements might be partially satisfied because of the use of small aggregate in the microconcrete, the cement particle size cannot be scaled. In other words, a precise simulation of a small-scale model concrete is impossible. For this reason, selection of model materials in this study was done on a "practical" basis rather than on a "theoretical" basis.

The cement used for the prototype concrete cylinders was commercially available Portland cement, ASTM Type 1, supplied by the Alpha Portland Cement Co. of Syracuse, N.Y. The cement had 55.2% tricalcium silicate ($C_3S$), 8.2% tricalcium aluminate ($C_3A$), and a Blain fineness of 3750 cm/kg. The cement used for the micoconcrete cylinders was commercially available ASTM Type III.

Type III cement was selected for the microconcrete for several reasons: (a) it's more rapid curing greatly facilitated the testing of many model mixes, (b) the finer grinding of this cement provides particles that are smaller than in Type I, as desired from simitude considerations, and (c) previous studies showed that it was easier to obtain consistent results with this type of cement. Sand and gravel used were from a local quarry near Ithaca, N.Y. The sand consisted primarily of quartz; the larger particles contained some shale, sandstone, and limestone. The sand had a fineness modulus of 2.60 and an absorption of 1.85% by weight. The gravel was natural river stone with a maximum size of 3/4 inches. The gravel had an absorption of 0.39% by weight.

### 2.2.2  Concrete Mixes

The mixes used to cast the cylinders were developed from existing data compiled earlier at Cornell University and through extensive trial batching. The mixes used for both the prototype and the microconcretes were designed to develop a cylinder compressive strength of 4500 psi, which was considered to be a common concrete strength.

The five different mixes were used in making the test cylinders are defined in Table 2.1.

Sand, which is defined as having aggregate particles smaller than #4 U.S. standard sieve was purchased from a local aggregate stone company. In selecting the sand, primary attention was given to getting uniformly graded sand as shown by Curve 1 in Figure 2.1. The gradation curve of the gravel is given by Curve 2.

For the prototype concrete, the originally obtained sand and gravel were mixed by the weight ratio of 3 to 3, with the resulting gradation curve as given by Curve 3 in Figure 2.1.

The microconcretes used only sand and cement without any gravel. In order to get variously graded sands for the microconcretes, the sand was divided into two parts; one had particles larger than #8 sieve size and smaller than #4 sieve size(called model gravel) and denoted by $G_m$ in this study. The other fraction had particles smaller than #8 sieve size (called model sand) and denoted by $S_m$ as shown in Figure 2.1. Sands having different gradation curves were made by re-combining the model sand and the model gravel with different mix ratio.

For Microconcretes I and II, the original sand was used with a sand to cement ratio of 3 and a sand to gravel ratio of 4. In Microconcrete II the coarse particles corresponding to the model gravel size were coated with poly-stylene. This was done to reduce model concrete tensile strength by reducing the bond strength between the cement paste and the coarse aggregate [9]. One-eighth diameter, high polymer polystylene pellets were added to commercial grade toluene to give a 10% solution by weight. The solution was kept in a sealed container to prevent evaporation of the toluene. The model gravel to be coated was thoroughly washed, then oven dried at 110°C for one day to remove the hydroscopic moisture, and then allowed to cool. The model gravel was completely submerged in the polystylene solution two times, being allowed to drain and dry completely between each application. Then the coated model gravel was mixed with the model sand to make Microconcrete II. The aggregate used for Microconcrete III consisted of the model sand and gravel in a mix ratio of 3 to 3 in order to increase the portion of large particles. To further increase the portion of large particles, the model sand and gravel were mixed in a ratio of 2 to 4, in Microconcrete IV. The gradation curves of the aggregate used for Microconcretes III and IV are represented by Curves 4 and 5, respectively, in Figure 2.1.

TABLE 2.1  MIX RATIOS OF TEST SPECIMENS

------------------------------------------------------------------------

| Mix | Water | Cement | Sand(Sm+Gm)* | Coarse Aggregate |
|-----|-------|--------|--------------|------------------|
| Prototype Concrete | 0.65 | 1 | 3(2.4+0.6) | 3 |
| Microconcrete I | 0.70 | 1 | 3(2.4+0.6) | 0 |
| Microconcrete II | 0.70 | 1 | 3(2.4+0.6)** | 0 |
| Microconcrete III | 0.70 | 1 | 6(3.0+3.0) | 0 |
| Microconcrete IV | 0.70 | 1 | 6(2.0+4.0) | 0 |

------------------------------------------------------------------------

Note:   * Sm; Model sand defined by particle size smaller than #8 seive

Gm; Model gravel defined by particle size larger than #8

seive and small than #4 seive

** Gm  in this mix was coated by a chemical material.
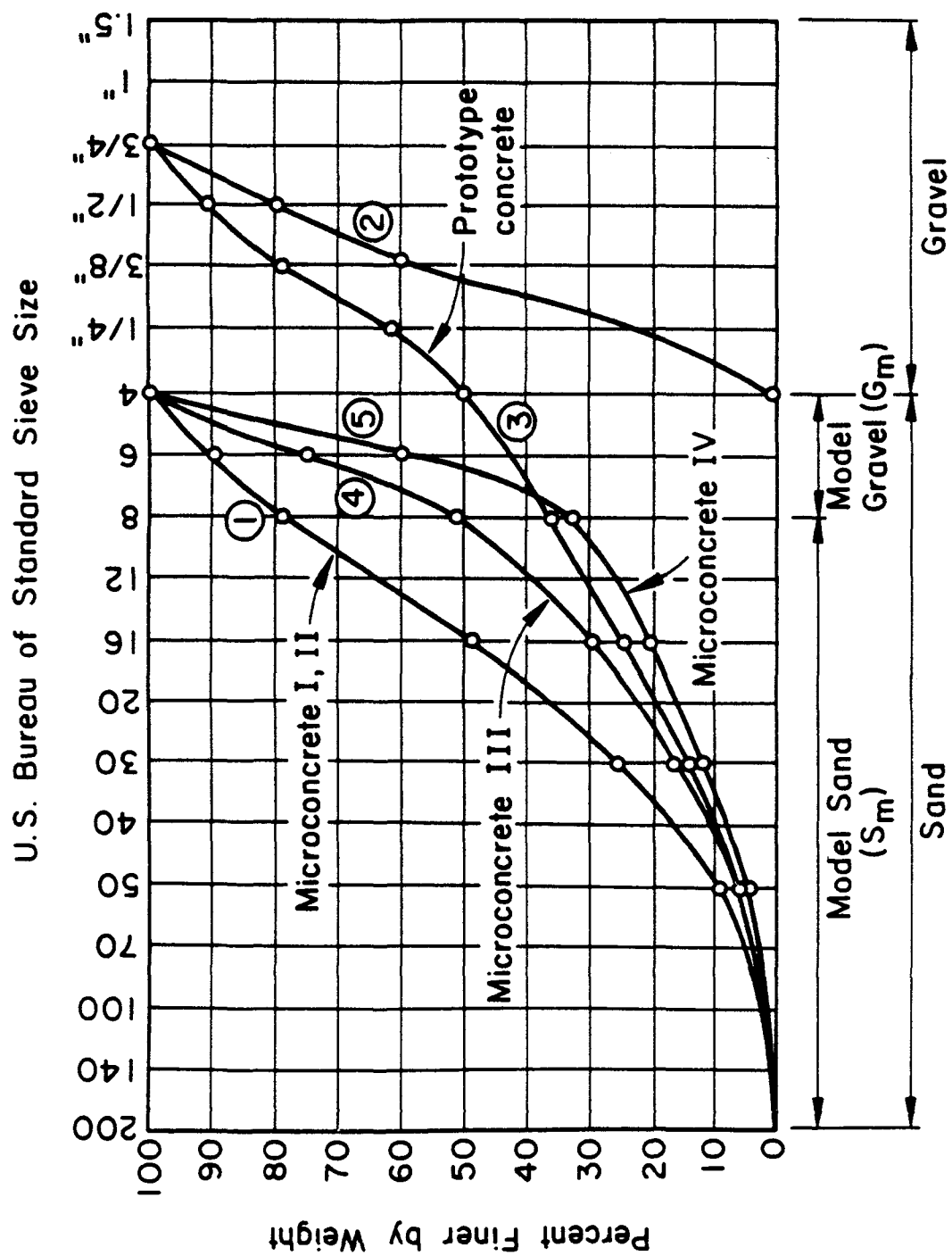
Figure 2.1. Grading Curves of Aggregate Used.

### 2.2.3 Specimen Preparation

For each concrete, 14 test cylinders were made from one batch (7 for compressive tests and the other 7 for split tensile tests).

Two by four inch cylinders were cast for the measurement of the micro-concrete properties. Existing steel laboratory forms were used, and a small hobart mixer was employed. Each model test cylinder was compacted for several minutes on an electric vibrating table. Six by twelve inch standard test cylinders were prepared for the prototype concrete. Disposal commercial forms were used. A 3.5 cu. ft. capacity tilt rotating mixer and an electric vibrating rod were employed in mixing and compacting the prototype concrete.

The forms were removed one day after casting, and specimens were immersed in water for two weeks until testing.

### 2.2.4 Instrumentation and Loading

A hydraulic, servo-controlled MTS structural Test System was used for loading. Load was applied through a MTS hydraulic actuator having a capacity of 600 kips, with integral load cell and displacement monitor. The entire test was controlled by a Hewlett Packard (HP) 9825B calculator, and monitored by an automatic data acquisition system.

Compressive strain in the test cylinder was measured with an extensometer with a gage length equal to half the test cylinder height. The stroke of the actuator was programmed to increase linearly until the cylinder failed. The stress and strain were continually monitored, printed, and plotted on the screen of HP 9825B.

### 2.3 Test Results

The observed test data are summarized in Table 2.2. Although the results showed that the microconcretes had less stiffness, and larger compressive strain capacity than the prototype concrete, differences were minimized by appropriate adjustments to the model microconcrete mixes.

Table 2.2  Summary of Concrete Cylinder Tests

| Mix (W : C : S : A) | Compression Cylinder Tests | | | | Split Tensile Tests | | |
|---|---|---|---|---|---|---|---|
| | $f'_c$ (psi) | $e_u$ (in/in) | $E_{int}$ (ksi) | $E_{0.4f'_c}$ (ksi) | $f'_t$ (psi) | $f'_t/f'_c$ | $f'_t/\sqrt{f'_c}$ |
| Prototype Concrete (0.65:1:3:3) | 4870 | .00229 | 3686 | 3081 | 461 | 0.095 | 6.61 |
| Microconcrete I (0.7:1:3:0) | 4607 | .00345 | 1924 | 1767 | 518 | 0.112 | 7.63 |
| Microconcrete II (0.7:1:3:0) | 4250 | .00424 | 1771 | 1538 | 382 | 0.090 | 5.86 |
| Microconcrete III (0.7:1:6:0) | 4683 | .00301 | 2997 | 2399 | 449 | 0.096 | 6.56 |
| Microconcrete IV (0.7:1:6:0) | 5354 | .00293 | 3136 | 2485 | 379 | 0.071 | 5.17 |

Notes:  1.  For Prototype concrete, 6X12 inch standard cylinders were tested.

2.  For all Microconcretes, 2X4 inch model cylinders were tested.

3.  Various gradations of sand were used in the microconcretes (see Table 2.1).

### 2.3.1 Prototype Concrete

The average compressive cylinder strength from 5 test cylinders was 4870 psi. As shown in Figure 2.2, compressive stress-strain relationship, strain at maximum stress ($e_u$), and secant modulus of elasticity at both initial and 0.4 $f_c'$ were obtained. The average value of the strain at maximum stress was 0.00229. Furthermore, five split cylinder tests were conducted to determine an average split tensile strength of 461 psi with a deviation of 29 psi. Expressed in terms of $f_c'$, the prototype concrete tensile strength is 0.095 $f_c'$ or 6.61 $\sqrt{f_c'}$. These values are considered as typical common prototype concretes used in practice, and are used here as a basis for comparison with the microconcrete properties.

### 2.3.2 Microconcrete I

Figure 2.3 shows the results obtained from testing 2x4 inch model concrete cylinders of Microconcrete I. The data scatter may be partially due to the use of a testing machine with a very large capacity on the small cylinders. Compared to the prototype concrete, the strain of Microconcrete I at maximum stress was 50% larger. Microconcrete I was much softer, as indicated by $E_{int}$ and $E_{0.4}$ in the table of Figure 2.3. The average split tensile strength was 518 psi with a standard deviation of 58 psi. In terms of the ratio of $f_t'$ to $f_c'$, Microconcrete I had a tensile strength 18% higher than the prototype concrete.

### 2.3.3 Microconcrete II

Since the model gravel used in Microconcrete II was coated with plastic to reduce the bond strength between the cement paste and the coarse aggregate, the tensile strength was significantly reduced. The average split tensile strength of Microconcrete II was 5% smaller than that of the prototype concrete, and 20% smaller than that of Microconcrete I. However, the strain at maximum stress was almost two times larger than that of the prototype concrete as shown in Figure 2.4. The aggregate coating in Microconcrete II provided a soft layer with reduced bond strength and a greatly decreased overall stiffness.

It may be concluded that by coating coarse aggregate, the excessive tensile strength of normal microconcrete is eliminated, but the modulus stiffness becomes too low, leading to a strain distortion that would be particularly objectionable in dynamic modeling.

# Normalized Stress-Strain Curves



Prototype concrete

--- Test results

— Average stress-strain curve.

Mix ratio W:C:S($S_m$+$A_m$):A =.65:1:3:3

| | $f_c'$ (psi) | e @ $f_c'$ (in/in) | Eint (ksi) | E @ .4$f_c'$ (ksi) |
|---|---|---|---|---|
| 1 | 4911 | .00222 | 3,622 | 3,174 |
| 2 | 4832 | .00237 | 3,945 | 3,182 |
| 3 | 4828 | .00224 | 3,363 | 3,203 |
| 4 | 4927 | .00229 | 3,773 | 2,901 |
| 5 | 4851 | .00235 | 3,726 | 2,943 |
| mean | 4870 | .00229 | 3,686 | 3,081 |

| | $f_t'$ (psi) | $f_t'$ /$f_c'$ |
|---|---|---|
| 1 | 509 | .104 |
| 2 | 457 | .094 |
| 3 | 476 | .098 |
| 4 | 433 | .089 |
| 5 | 431 | .089 |
| mean | 461 | .095 |
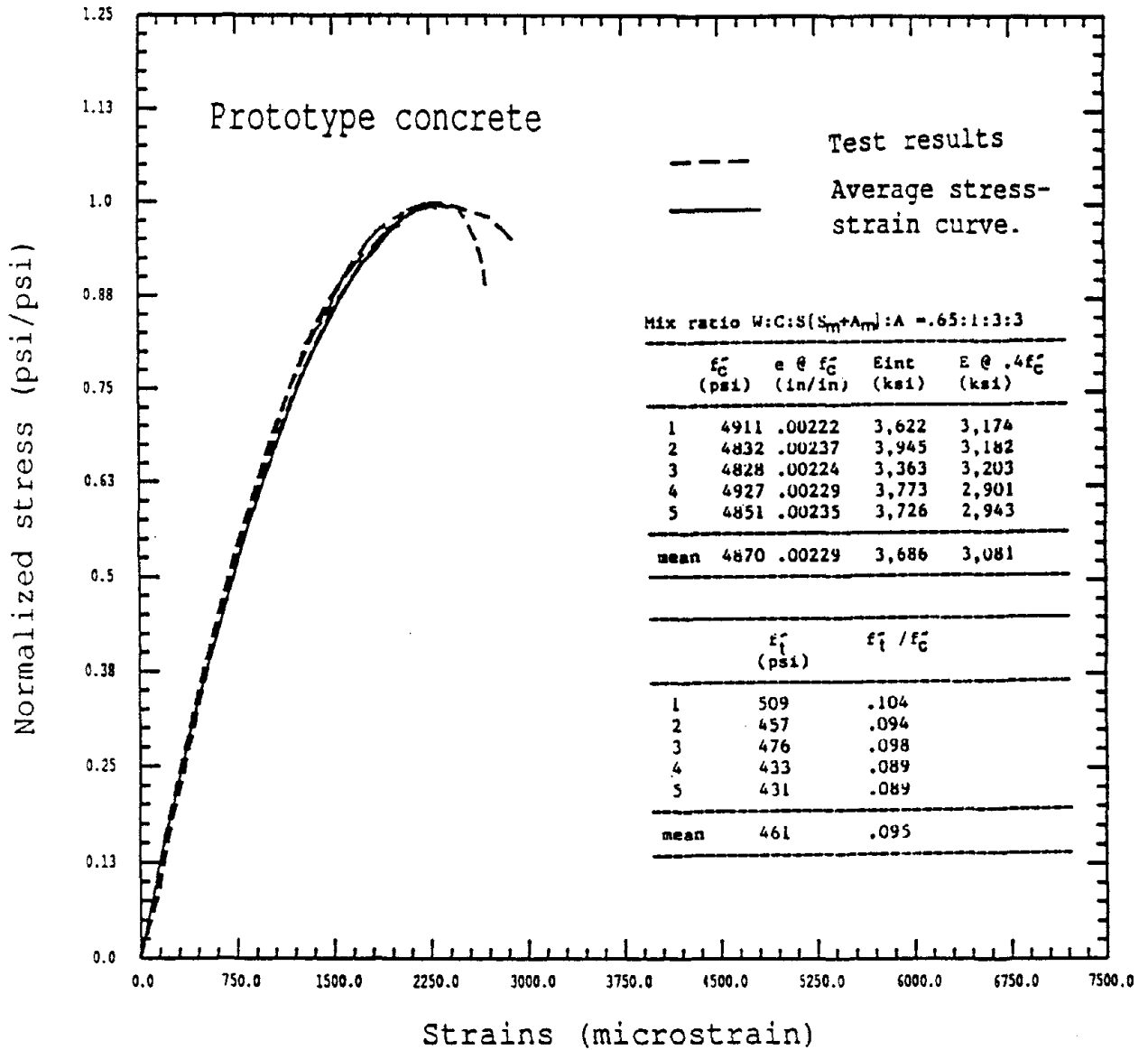
Fig. 2.2   Prototype concrete

# Normalized Stress-Strain Curves

Microconcrete I

W:C:S($S_m$+$A_m$):S = .7:1:3[2.4+0.6]:0

| | $f_c'$ | e @ $f_c'$ | Eint | E @ .4$f_c'$ |
|---|---|---|---|---|
| 1 | 4783 | .00329 | 2,108 | 2,091 |
| 2 | 4912 | .00366 | 1,988 | 1,870 |
| 3 | 4636 | .00392 | 1,553 | 1,395 |
| 4 | 4236 | .00324 | 1,587 | 1,591 |
| 5 | 4467 | .00313 | 2,383 | 1,886 |
| mean | 4607 | .00345 | 1,924 | 1,767 |

| | $f_t'$ | $f_t'$ /$f_c'$ |
|---|---|---|
| 1 | 604 | .131 |
| 2 | 514 | .112 |
| 3 | 440 | .095 |
| 4 | 473 | .103 |
| 5 | 559 | .121 |
| mean | 518 | .112 |

Normalized stress (psi/psi)

Strains (microstrain)
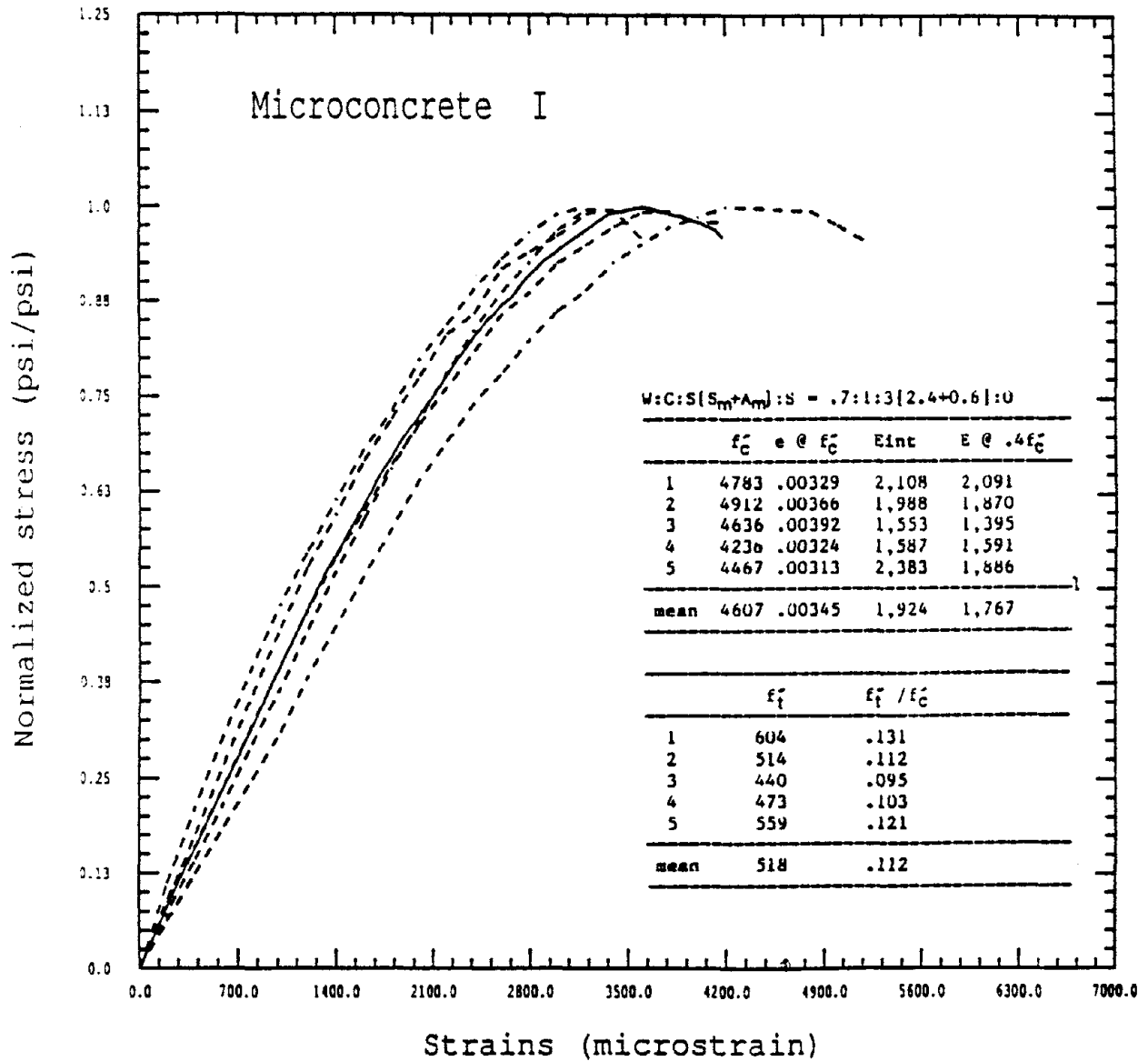
Fig. 2.3  Microconcrete I

## Normalized Stress-Strain Curves



Microconcrete II
(With Coated Gravel Particles)

$W:C:S[S_m+A_m]:A = .7:1:3[2.4+0.6]:0$

|   | $f'_c$ | $e @ f'_c$ | Eint | $E @ .4f'_c$ |
|---|---|---|---|---|
| 1 | 5186 | .00421 | 1,971 | 1,713 |
| 2 | 4084 | .00512 | 1,062 | 0,989 |
| 3 | 4025 | .00380 | 2,279 | 1,913 |
| 4 | 3904 | .00395 | — | — |
| 5 | 4049 | — | — | — |
| mean | 4250 | .00425 | 1,771 | 1,538 |

|   | $f'_t$ | $f'_t / f'_c$ |
|---|---|---|
| 1 | 369 | .087 |
| 2 | 388 | .091 |
| 3 | .423 | .099 |
| 4 | 336 | .079 |
| 5 | 392 | .092 |
| mean | 382 | .090 |
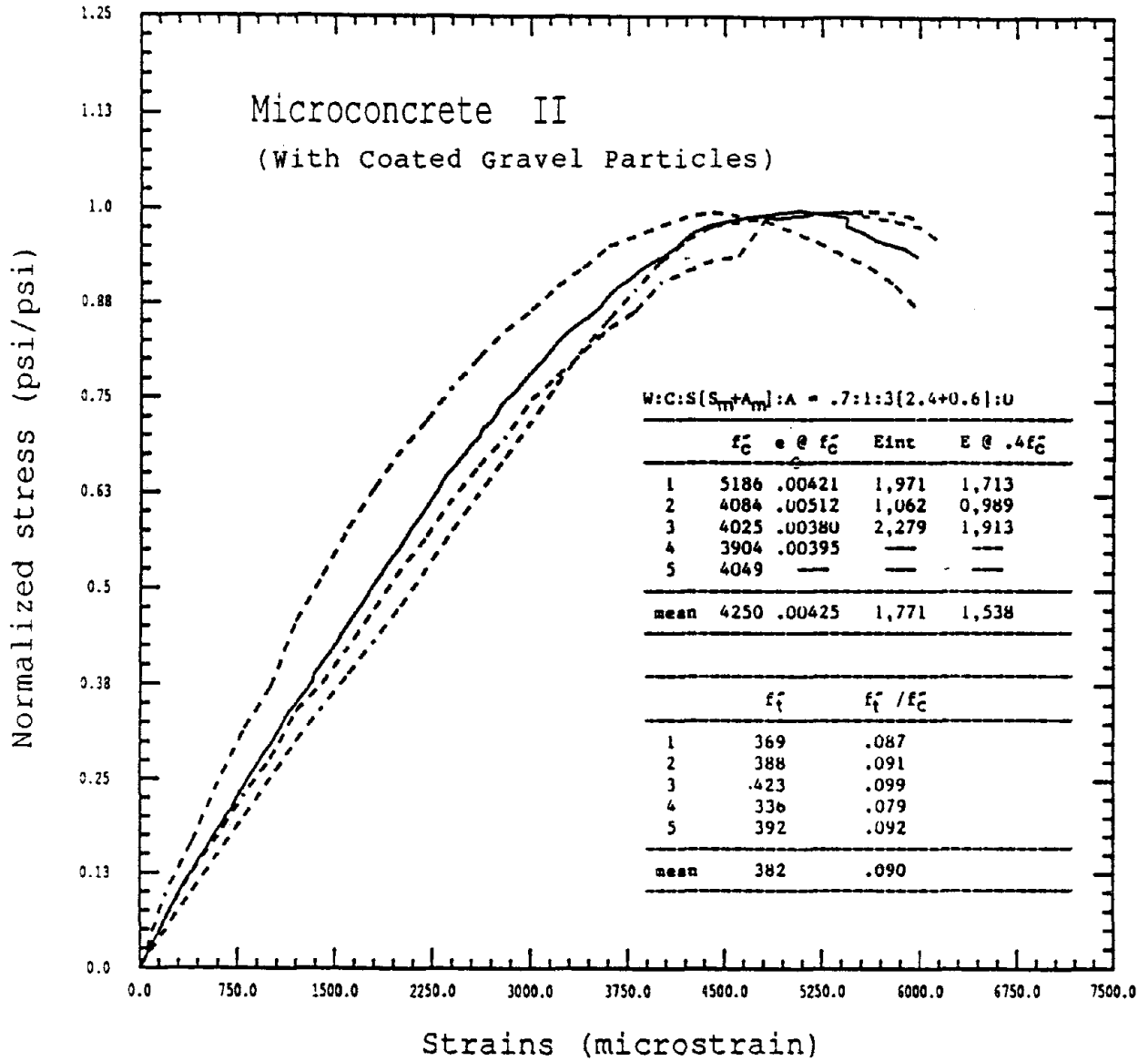
Fig. 2.4   Microconcrete II

### 2.3.4 Microconcrete III

The compressive stress-strain curves and basic properties of Microconcrete III are presented in Figure 2.5. The average split tensile strength was 449 psi. The ratio of $f_t'/f_c'$ was 0.096 which was very close to the 0.095 ratio of the prototype concrete. The average strain at $f_c'$ was 0.00301, 31% larger than $e_u$ of the prototype concrete. This implied that Microconcrete III was still less stiff. Compared to Microconcrete I, however, Microconcrete III was much improved with respect to stiffness and tensile strength.

Since aggregate itself is stiffer than cement paste, the stiffness of concrete increases as the portion of aggregate in the mixture increases. However, decreases in the ratio of aggregate to cement (A/C) and the ratio of water to cement (W/C) were limited due to workability requirements. In the present work, it was observed that the A/C of 6 with W/C of 0.7 was the mixture which provided minimum acceptable workability with the additive of a normal amount of superplasticizers.

### 2.3.5 Microconcrete IV

The ratio of A/C in Microconcrete IV was the same as in Microconcrete III(6), but the gradation of the aggregate was different (1:2 rather than 1:1). Thus Microconcrete IV resulted in higher stiffness than Microconcrete III. The average strain at $f_c'$ was 0.00293, 27% higher than $e_u$ of the prototype concrete as presented in Figure 2.6.

The average split tensile strength as a function of $f_t'/f_c'$ was 0.071, 25% lower than that of the prototype concrete. This was mainly attributed to excessive honeycombing which resulted from using the rather poorly graded aggregate. During casting, it was difficult to compact specimens because of bad workability, even though a normal amount of superplasticizers was used.

### 2.4    Summary and Conclusion

Various microconcrete mixtures were studied to obtain a better practical model concrete for small-scale model experiments on reinforced concrete structures. The main aspects considered here were (1) reducing the excessive tensile strength, and (2) increasing the stiffness of the microconcrete.

## Normalized Stress-Strain Curves



**Microconcrete III**

Axis labels: Normalized stress (psi/psi) vs Strains (microstrain)

W:C:S($S_m$+$A_m$):A = .7:1:6(3+3):0

| | $f'_c$ | e @ $f'_c$ | Eint | E @ .4$f'_c$ |
|---|---|---|---|---|
| 1 | 4816 | .00218 | 3,221 | 2,498 |
| 2 | 4824 | .00282 | 2,563 | 2,557 |
| 3 | 4896 | .00309 | 3,184 | 2,342 |
| 4 | 4758 | .00312 | 3,439 | 2,157 |
| 5 | 4431 | .00294 | 3,372 | 2,676 |
| 6 | 4377 | .00296 | 2,202 | 2,163 |
| mean | 4683 | .00301 | 2,997 | 2,399 |

| | $f'_t$ | $f'_t$ /$f'_c$ |
|---|---|---|
| 1 | 313 | .067 |
| 2 | 421 | .090 |
| 3 | 399 | .085 |
| 4 | 576 | .123 |
| 5 | 536 | .114 |
| mean | 449 | .096 |
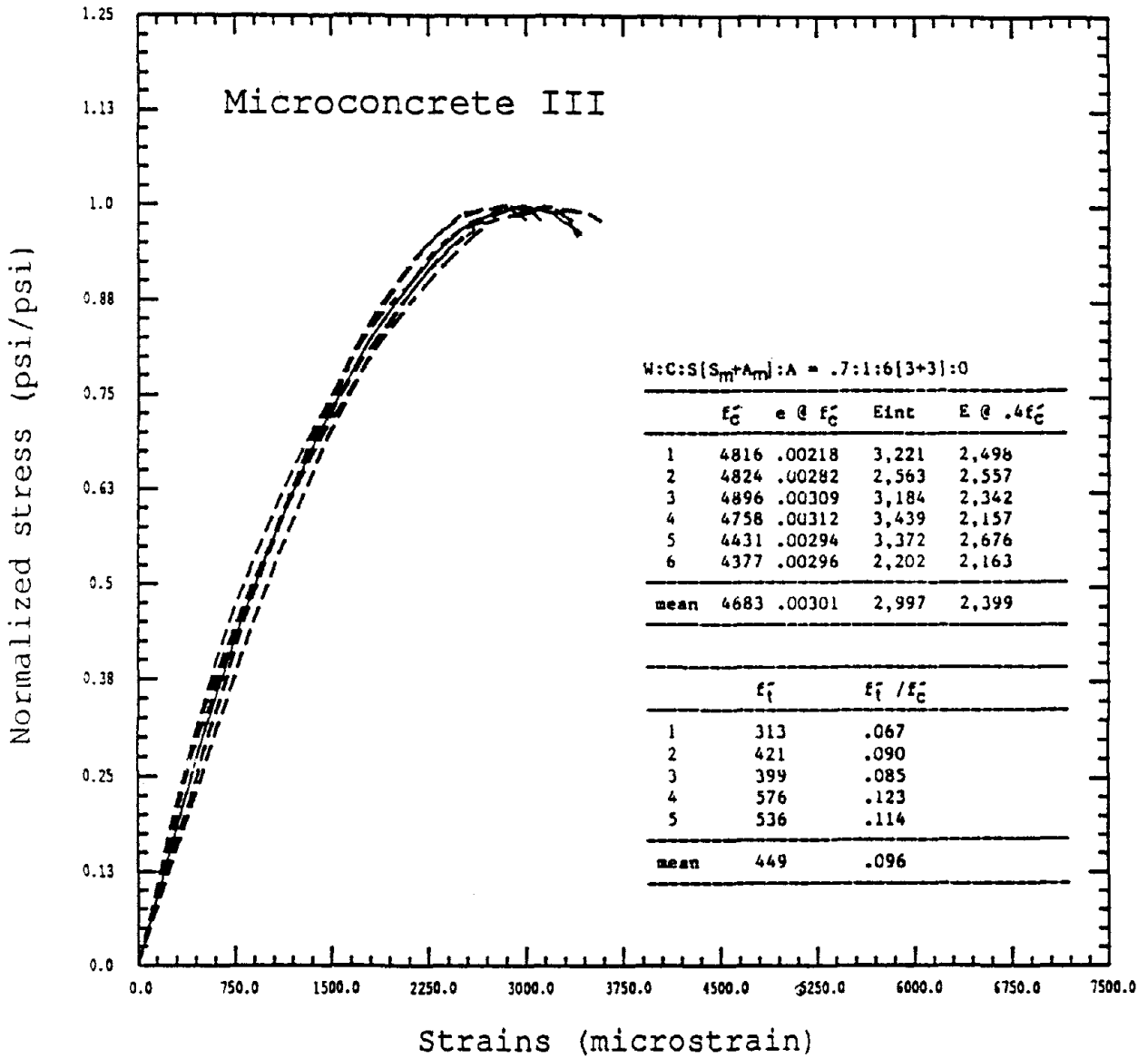
Fig. 2.5  Microconcrete III

## Normalized Stress-Strain Curves



Microconcrete IV

W:C:S(S_m+A_m):A = .7:1:6(2+4):0

| | $f'_c$ | $e$ @ $f'_c$ | Eint | E @ .4$f'_c$ |
|---|---|---|---|---|
| 1 | 5023 | .00294 | 3,381 | 2,541 |
| 2 | 5192 | .00259 | 3,824 | 2,536 |
| 3 | 6003 | .00326 | 3,168 | 2,241 |
| 4 | 5338 | .00320 | 2,741 | 2,357 |
| 5 | 5466 | .00277 | 3,145 | 2,578 |
| 6 | 5104 | .00286 | 2,554 | 2,657 |
| mean | 5354 | .00293 | 3,136 | 2,485 |

| | $f'_t$ | $f'_t$ /$f'_c$ |
|---|---|---|
| 1 | 343 | .064 |
| 2 | 317 | .059 |
| 3 | 346 | .065 |
| 4 | 329 | .061 |
| 5 | 559 | .104 |
| mean | 379 | .071 |
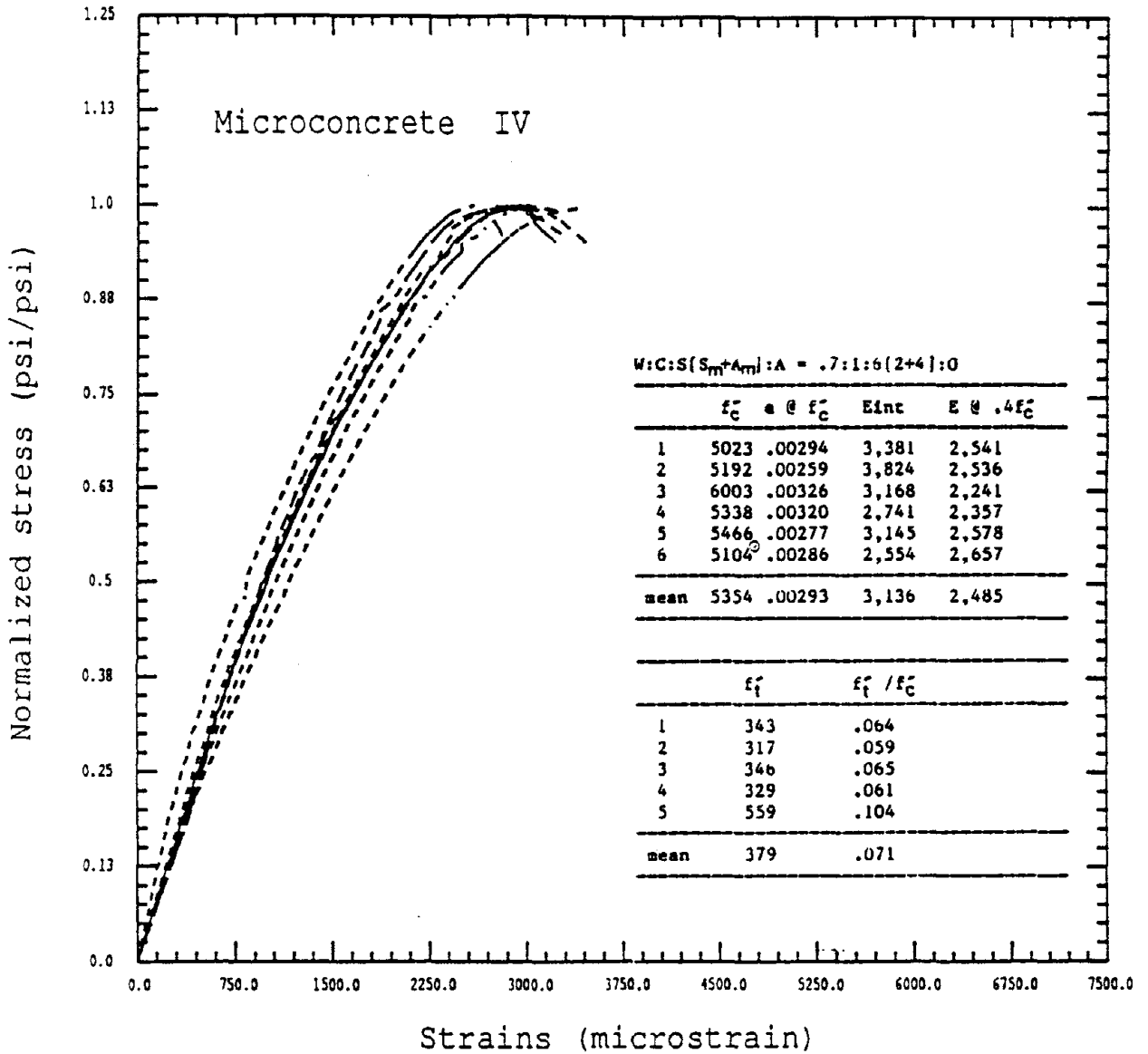
Fig. 2.6    Microconcrete IV

2-14

One prototype concrete and four microconcretes were tested. The results obtained are summarized in Table 2.2, and the normalized average compressive stress-strain curves are compared in Figure 2.7.

Based on the supposition that concrete tensile strength is mainly dependent on the bond resistance between cement paste and aggregates, the coarse aggregates in Microconcrete II were coated with plastic to reduce the normally high tensile strength of a microconcrete. Although the tensile strength was reduced successfully, the compressive stiffness became too low as shown in Figure 2.7.

The ratio of A/C was then chosen as the primary variable to control the microconcrete properties. The results showed that as the ratio of A/C increases, the compressive stiffness increases, and tensile strength decreases. Since the aggregate is, in nature, much stiffer than cement paste, (Figure 2.8), it is natural that the stiffness of a concrete increases as A/C increases. In addition to this, the tensile strength decreases with increase of A/C ratio. The variation of the stiffness and $f_t'$ of microconcretes with respect to A/C ratio is shown in Figure 2.9.

It is concluded that Microconcrete III is the best mixture for dynamic experimental modeling of R/C structures.
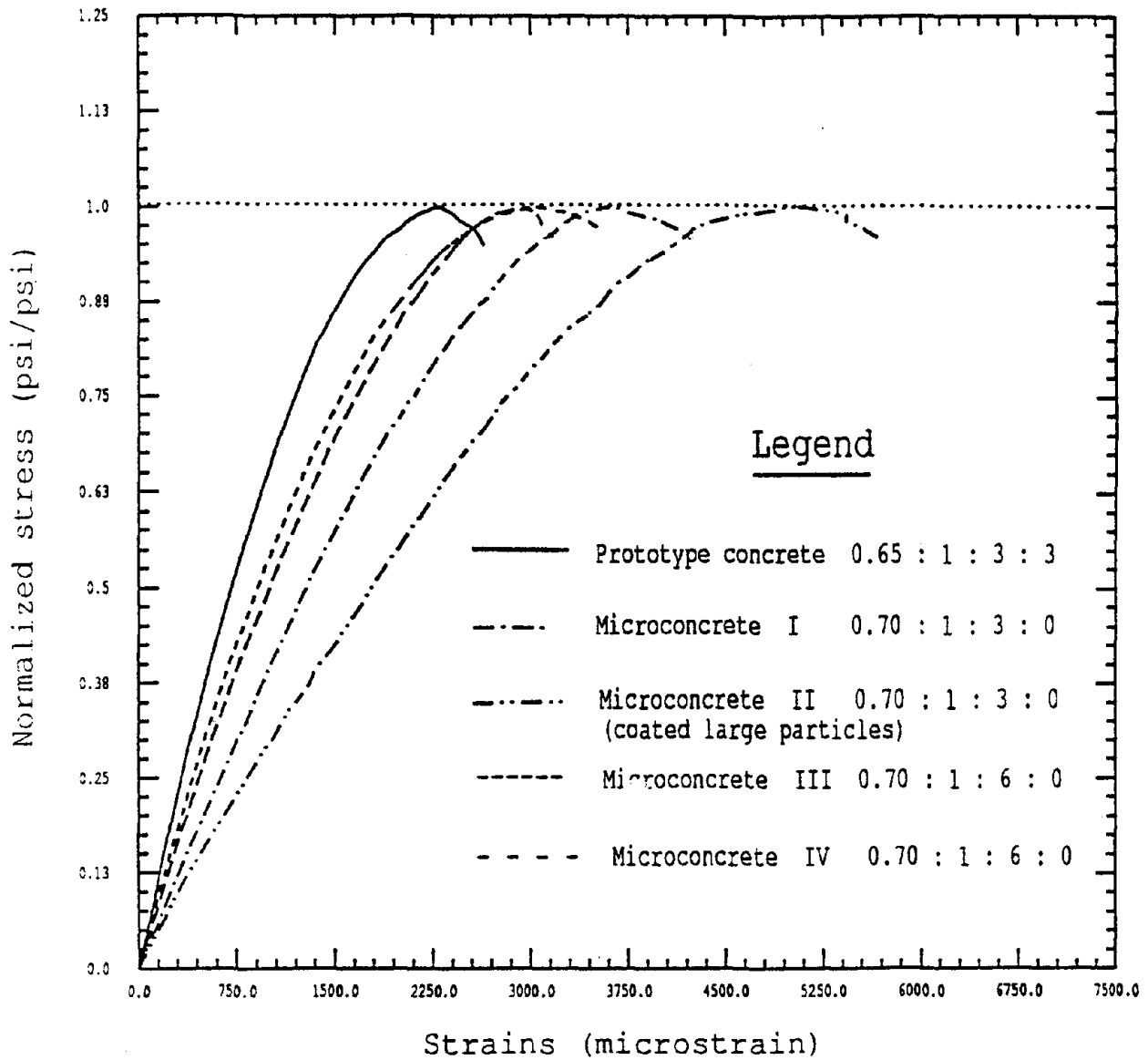
Fig. 2.7   Summary of Mean Normalized Stress-Strain
           Relationships of Concretes tested

2-16
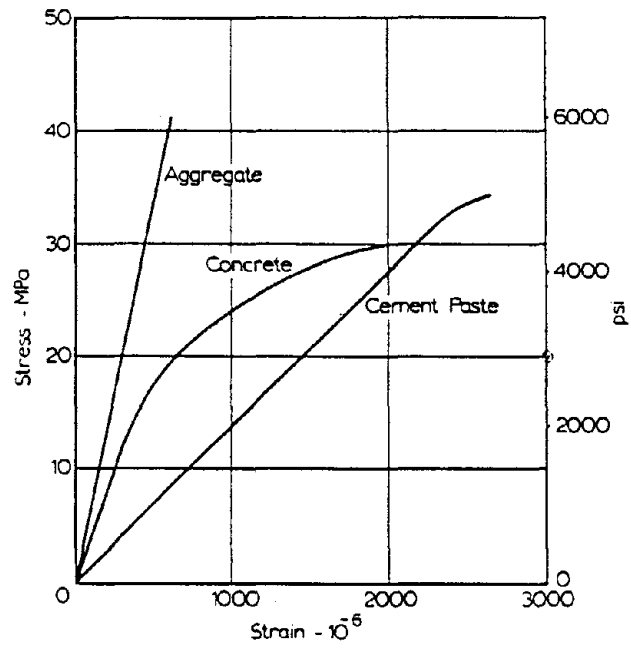
Fig. 2.8   Stress- strain Relations of
Aggregate, Concrete   and
Cement Paste
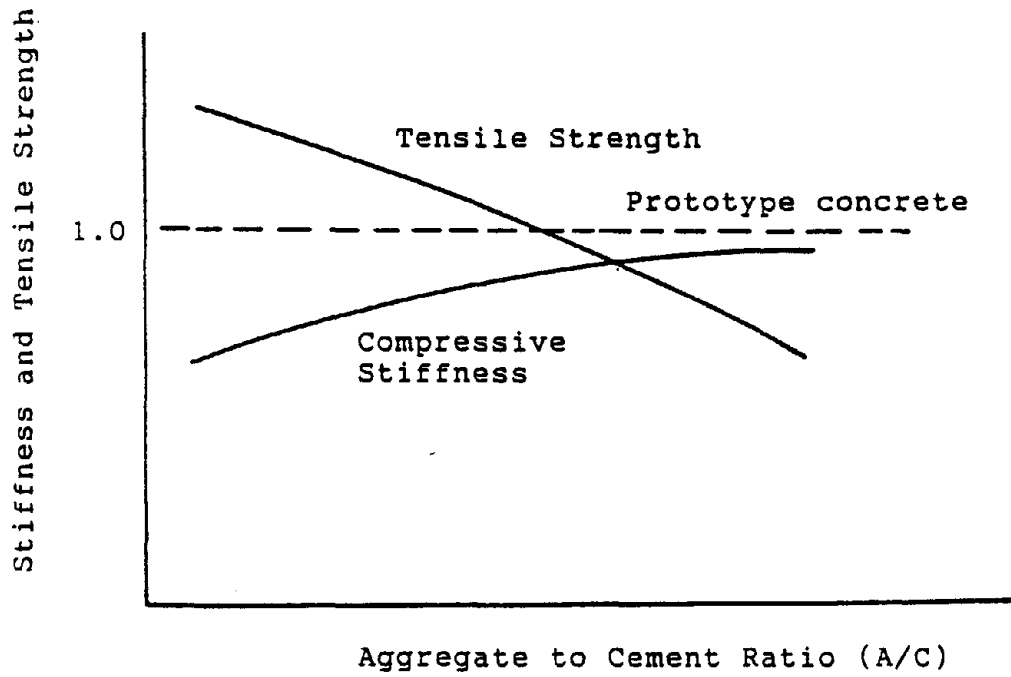
Fig. 2.9    Schematical Variation of Stiffness and
Tensile Strength of Microconcrete as
Function of A/C Ratio

# Chapter III
# MODEL REINFORCEMENT

## 3.1  Introduction

One of the main objectives of the present work was to reproduce the proto-type structure response at various stages of loading up to failure at model scale.  The considered range of loading covers the elastic, inelastic, and the ultimate stages of behavior.  Since most reinforced concrete elements are usually under- reinforced to provide sufficient ductility and to achieve an economical use of steel reinforcement, the post-yield stress-strain characteristics of both the prototype and model reinforcement are critical in determining the structural behavior in the inelastic cracked range.

Another important aspect of the selection of model reinforcement is the proper representation of bond.  Various techniques have been proposed by model investigators to improve the bond characteristics of model reinforcement for best cracking similitude.  Plain wires with rusted surfaces, cold-rolled threaded rods, deformed wires, etc. have been examined by many researchers [6,8].  However, a definitive solution of the model reinforcement problem, including bond, is not yet available.

## 3.2  Selection of Model Reinforcement

### 3.2.1 Bar Size

The choice of bar diameter was based on a 1/6 scale replica of the prototype reinforcement.  The exact required diameters were almost impossible to find in the market, but every attempt was made to obtain model bars with diameters as close as possible to the required sizes.  In some cases, such as when threaded bars were used, it was necessary to use a combination of small and large diameter wires.  This was done on the expense of slightly distorting the exact reproduc-tion of the total surface area of the prototype bars.  The cross sectional area of the knurled wires was obtained as follows:

Area = Weight of wire / (Density x Length)

## 3.2.2 Surface Deformation

Several forms of surface deformations are examined in the present invest-
igation to obtain the best correlation between model and prototype cracking
patterns. Four types of wires were used: (1) plain wires with no surface
deformations, (2) threaded rods, (3) commercially deformed wires, and (4)
standard deformed wires. Main mechanical and surface properties of these
reinforcing wires are shown in Table (3.1), and figure (3.1) respectively.

The normally accepted state-of-the-art in model reinforcement representa-
tion is the use of deformed wires with surface deformations resembling those of
the prototype but at model scale. These so-called standard deformed wires were
obtained by knurling plain round wires using a device developed by H. G. Harris
at Drexel University. The knurling process resulted in raising the plain bars
yield strength by about 5%, and narrowing its yield plateau (Figure 3.2).

## 3.2.3 Mechanical Properties

Figure 3.2 shows the stress-strain curves of the as-delivered model rein-
forcement. It can be seen that all bars did not show a clearly defined yield
point. Also, commercially deformed wires (and to some extent the standard
deformed wires) had limited ductility. All model bars were heat-treated as
described in Section 3.3, to produce a sharp yield point and to develop the yield
strengths given in Table 3.2.

## 3.3 Heat Treatment

## 3.3.1 General

Heat treatment seems to be an essential process for proper simulation of
reinforcing steel. Model bars will rarely have either the desired yield strength
or sufficient ductility (yield plateau). Also, when smooth bars are cold-formed
to produce the required surface deformation, their yield strength increases while
their ductility decreases. This can be attributed to the state of high internal
strain produced by cold-forming [11]. Heat treatment or annealing of model bars
is used to control the yield strength, and to improve the yield and post-yield
characteristics, such as developing a clear sharp yielding point and increasing
the ductility.

TABLE 3.1  MODEL REINFORCING MATERIALS FOR TEST

| Type of Bar/Wire | | Physical Diameter (in.) | Nominal Diameter (in.) | Cross Sectional Area (in2) | Yield Strength as Delivered (ksi) |
|---|---|---|---|---|---|
| Smooth | | 0.120 | 0.120 | 0.0113 | 105 |
| Standard Deformed | | | 0.116 | 0.0105 | 110 |
| Commercially Deformed Wires | | | 0.114 | 0.0102 | 83 |
| Threaded | Small | 0.125(O.D.) 0.098(I.D.) | 0.107 | 0.0079 | 100 |
| | Large | 0.164(O.D.) 0.130(I.D.) | 0.133 | 0.0139 | 99 |
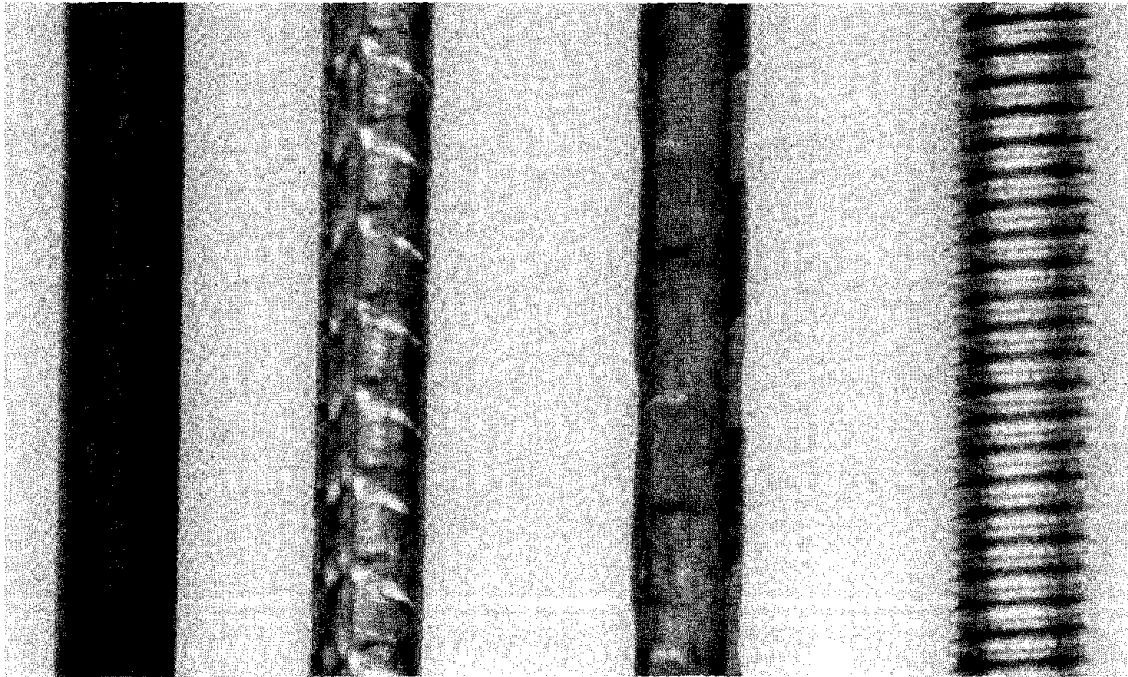
(a)        (b)        (c)        (d)

(a) Smooth Wire
(b) Standard Deformed Bar
(c) Lightly Deformed Model Bar
(d) Threaded Rod

Figure 3.1. Surface Deformation of Model
Reinforcement.
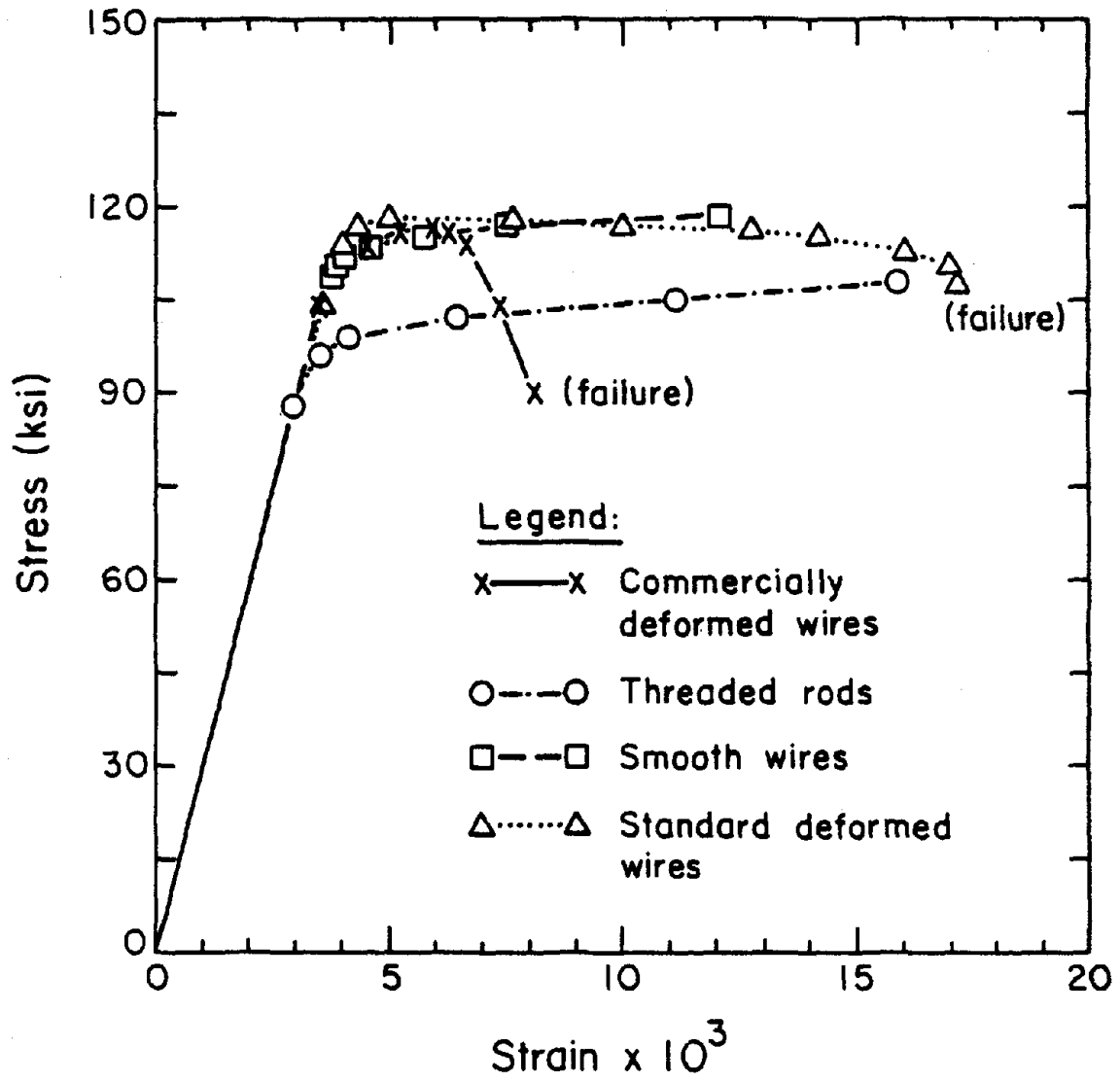
Figure 3.2. Stress-Strain Curves of Model
Reinforcement as Delivered.

Table 3.2 Annealing Results

| Bar Type | Strength as Delivered (ksi) | Required Strength (ksi) | Annealing Temperature (C) | Annealing Time (min) | Cooling Time (hr) | Annealed Bar Strength (ksi) | Ratio of Actual to Required Strength |
|---|---|---|---|---|---|---|---|
| Smooth Bars | 112 | 67 | 625 | 10 | —* | 67.7 | 1.01 |
| Standard Deformed | 110 | 75 | 540 | 10 | 1 1/2** | 77.3 | 1.031 |
| Commercially Deformed | 83 | 78 | 500 | 10 | 1 1/2** | 80.5 | 1.032 |
| Threaded Rods | 100 | 69 | 625 | 10 | 1 1/2** | 70.5 | 1.022 |

* Open tube (furnace B) was used.

** Vacuum tube (furnace A) was used.

The annealing process can be divided into three distinctive regions: recovery or strain relieving, recrystallization, and grain growth (Figure 3.3) [11]. At the recovery stage, the metal restores its physical properties without any significant change in its microstructure. Sharp yielding point can be obtained at this stage by annealing the steel to 340 C for about 2-3 hours. Recrystallization, (which is usually defined as conventional annealing) is the replacement of the cold worked structure by a new set of strain-free grains. From the different possible combinations of temperature and time used for conventional annealing, a temperature of 540 C for various time periods is recommended in reference [11] for typical steels.

### 3.3.2. Furnaces Used for Annealing

Two Lindberg electric furnaces located in the Cornell Materials Science and Engineering laboratory were used in the annealing process. The first (Furnace A, Figure 3.4) was a vacuum tube furnace with a digital thermocouple temperature control. The furnace body was divided into three zones which can be controlled separately. The thermocouple control system was designed to give the average temperature inside the furnace. Maximum temperature that could be attained using this furnace was 1200 C. The second furnace (Furnace B, Figure 3.4) was similar to the first furnace but with an open tube. Comparison between the performance of the two furnaces is discussed in Sections 3.3.4 and 3.3.5.

### 3.3.3 Annealing Processes

The main factors affecting the heat-treatment process are: annealing time, annealing temperature, rate of cooling, and temperature distribution inside the furnace. While the first two factors are the control parameters in this process, the last two are furnace dependent. Prior experience at Cornell indicated that a slight non-uniformity of temperature distribution inside the furnace may significantly affect the annealing results. To study this effect, each test specimen was cut into at least two pieces, and each piece was tested to verify a uniform yield strength all over the specimen length.

The annealing process using Furnace A was carried out as follows:

1. The steel specimen was placed inside the vacuum tube, and the tube was mounted on the furnace body.

3-7

Recovery  Recrystallization  Grain Growth

1. Grain Size
2. Ductility
3. Internal Strain
4. Strength

1
2
3
4

Temperature
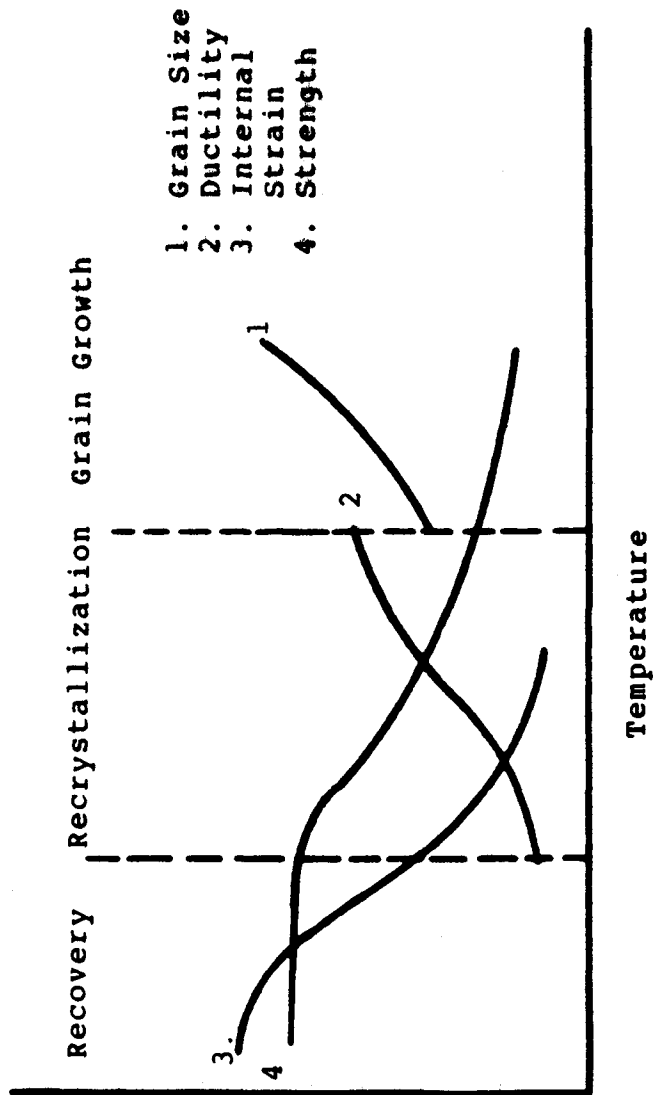
Figure 3.3. Schematic Drawing indicating Recovery, Recrystallization, and Grain Growth and Chief Property Changes in Each Region [11].

Zone(3) Zone(2) Zone(1)

Vacuum tube

Steel specimen

Heating element
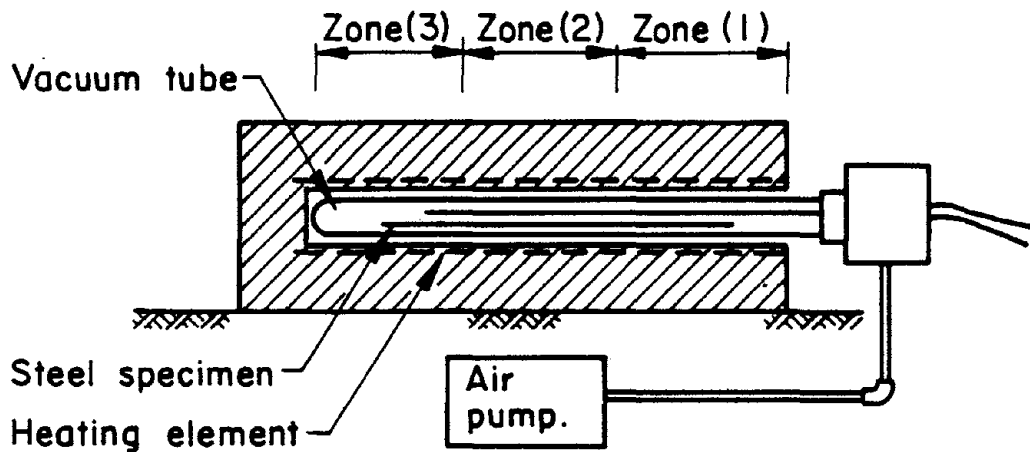
Air pump.

a) Furnace A: Vacuum Tube Furnace



Heating element

Zone(3) Zone(2) Zone(1)

Steel specimen
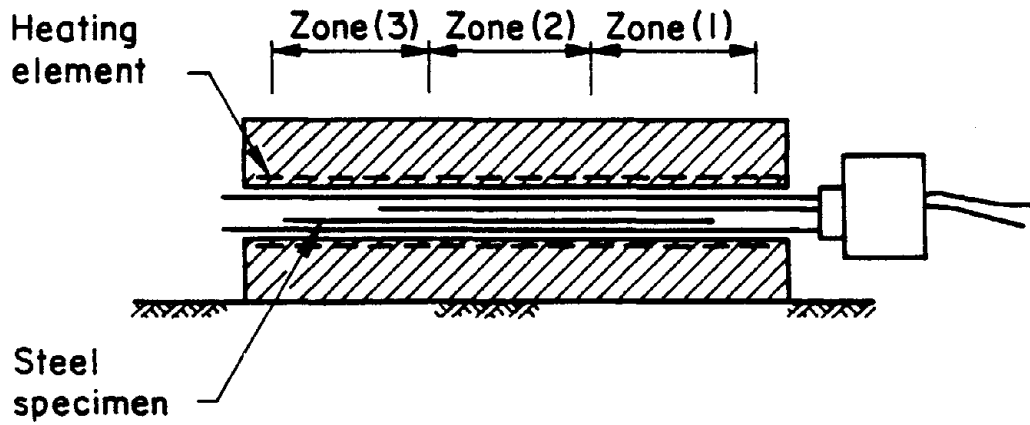
b) Furnace B: Open Tube Furnace

Figure 3.4. Furnaces Used For Heat Treatment.

2. The air was evacuated using an air pump, and the furnace was turned on.

3. After the required temperature was maintained for the desired annealing time (usually 10 minutes), the furnace was turned off and the specimen was left to cool inside the furnace for about 1-1/2 hrs.

4. The air valve was opened, and the specimen was taken out and tested.

The procedure used with furnace B was simpler than the above scheme. After the furnace was preheated to the required temperature, the steel specimens were placed inside it through the tube opening. The steel was then left inside the furnace for exactly the required annealing time and was then taken out to cool at room temperature.

Several advantages were observed when using furnace B (with an open tube). In addition to the easy placement of specimens inside the furnace, the temperature distribution inside the furnace was found to be more uniform than that of furnace A. Also, furnace B allows a precise time exposure to temperature since it was not necessary to leave the specimen inside the furnace during the heating and the cooling times. The color of specimens annealed in furnace B was changed (became darker) due to the oxidization of the surface layer of the steel bars. Since this had negligible contribution to the bond characteristics, the model bars were cleaned using only acetone after annealing.

### 3.3.4  Results of Selected Annealing Results

The annealing process using either furnace A or B was repeated several times to obtain the proper temperature and annealing time for each type of model bars. Figure 3.5 shows typical trial and error results of the heat-treatment of plain bars. Table 3.2 gives the annealing temperature and time used for each kind of model bars. Also, Figure 3.6 shows the stress-strain curves of the annealed bars. As given in Table 3.2, all the desired yield strengths were achieved with a maximum error of + 3.2%  A sharp, clearly defined yield point was obtained for all bars. The ductility of commercially deformed bars was improved due to heat-treatment.
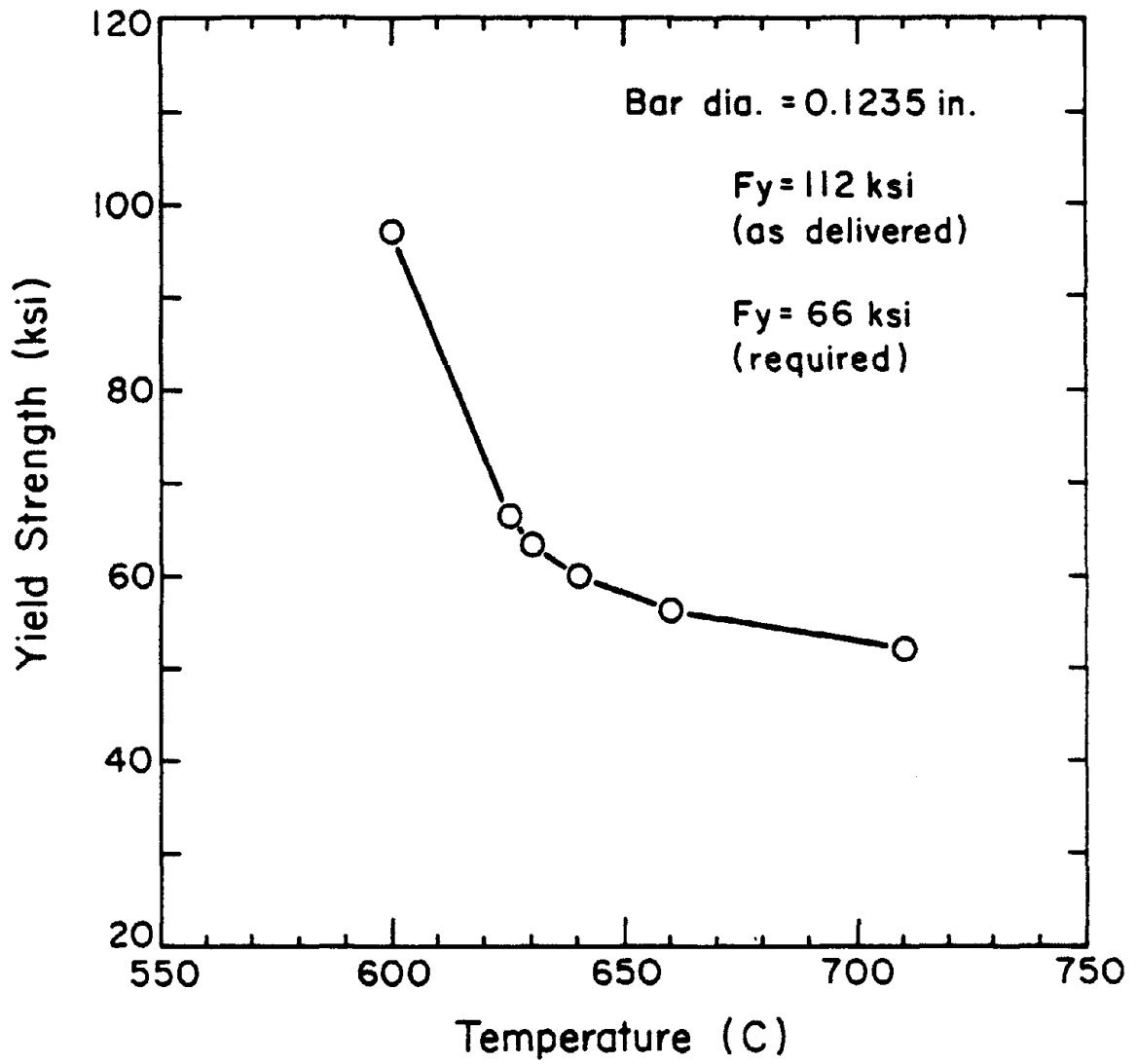
Figure 3.5. Heat Treatment of Plain Bars
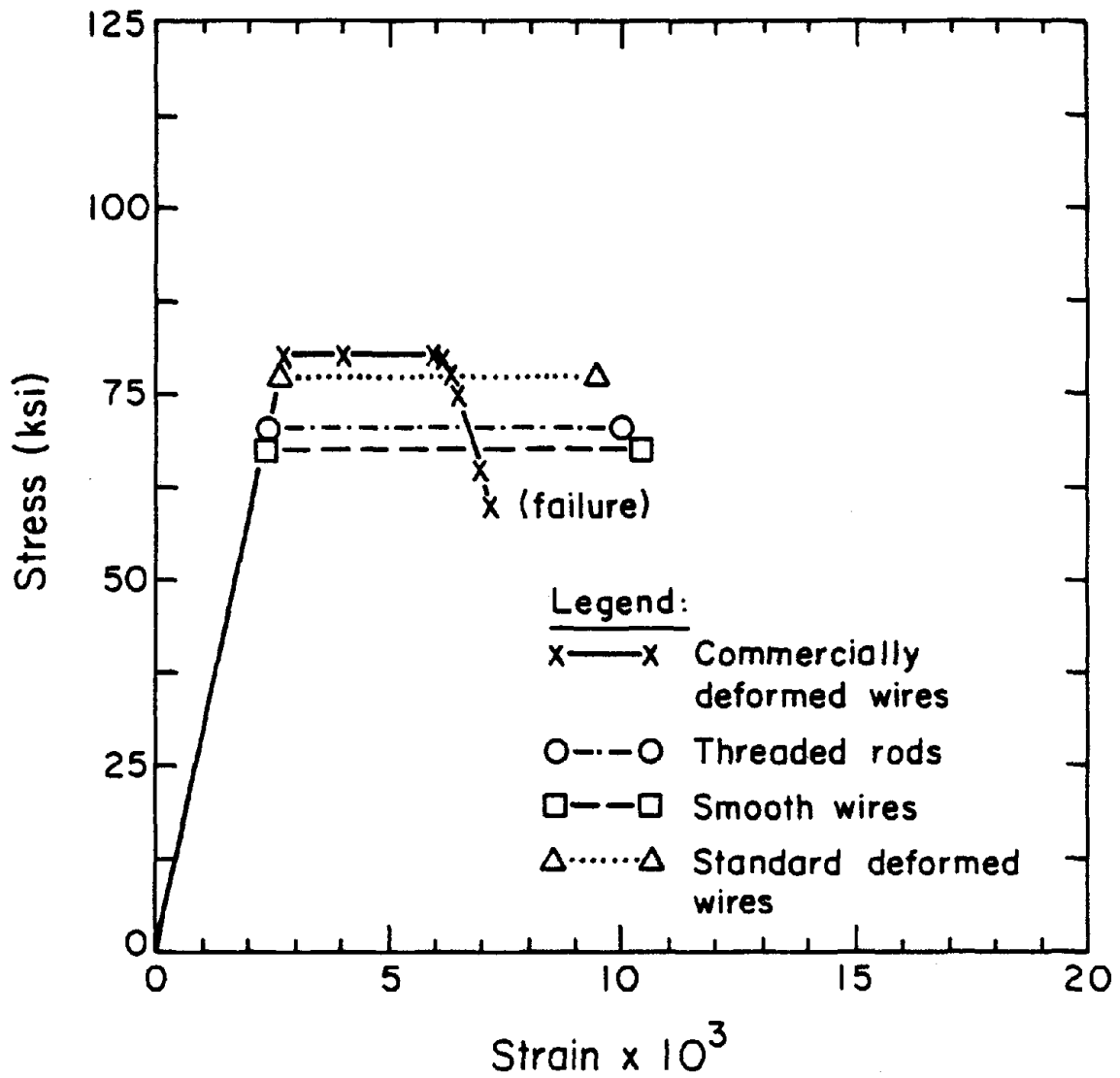
Figure 3.6. Stress-Strain Curves of Annealed Bars.

Two primary difficulties faced during the heat-treatment process: (1) obtaining a uniform temperature distribution inside the furnace (especially Furnace A), and (2) finding the proper combination of annealing temperature and time for different types of reinforcement using a certain furnace.

### 3.4 Summary and Conclusion

Several types of model reinforcement were heat-treated to develop the required yield strength, improve ductility, and obtain a sharp yield point. A trial and error approach was used to determine the proper annealing temperature and time for each model reinforcement to obtain the desired properties. It was found that the use of an open tube electric furnace offers many advantages, including accurate control of specimen exposure to the heating (temperature) process, uniform temperature distribution inside the furnace, and ease in moving specimens in and out of the furnace.

The annealing gave highly satisfactory results from the standpoint of achieving the desired yield strength. An annealing time of 1 hour is proposed for these wires. Heat-treatment did little to improve the ductility of the commercially deformed wires.

## CHAPTER IV
## HYSTERESIS RESPONSE OF MODEL REINFORCED CONCRETE BEAMS

### 4.1 Introduction

In addition to the physical characteristics of model concrete and reinforcement, other parameters should be considered for a thorough evaluation of whether similitude between model and prototype R/C response can be achieved.

State-of-the-art reviews of the response parameters of reduced scale reinforced concrete members indicates that particularly critical factors include bond characteristics and strain gradient effects. The bond characteristics between concrete and steel significantly affect cracking and, in particular, the post-yield response of a structure. Since bond-slip reduces the flexural stiffness and the dissipation of energy in hysteretic behavior, a lack of bond similitude between model and prototype has a correspondingly negative effect on similitude in structural damageability and collapse limit state responses. Furthermore, the strain gradient across a flexural member increases linearly with a decrease in size. since research indicates some dependence of concrete flexural strength with increasing strain gradient, some distortion of cracking might be expected.

In order to study the combined effect of bond and strain gradient on the hysteresis response of cyclically loaded reinforced concrete model structures, a prototype and several 1/6 scale model beams were tested under gradually increasing cyclic loads.

### 4.2 Test Program

### 4.2.1 Test Objectives and Variables

One prototype beam and three 1/6 scale model beams were tested. The prototype was used to provide a basis of critical comparison for the subsequent small scale model test results. The primary objective of the study was to ascertain the influence of model reinforcement with different surface deformation patterns on: (1) patterns and extent of concrete cracking, (2) overall hysteresis response, and (3) localized rotation characteristics at the section of highest flexure. This critical comparison could then be used to formulate recommendations as to the best type of model reinforcement for use in small scale modeling of reinforced concrete structures subjected to severe reversing loads.

The only variable studied with these model specimens was the type of surface deformation on the model reinforcement: none (smooth wire), standard deformed (scaled model of prototype reinforcement), and threaded.

### 4.2.2 Specimen Description and Materials

The test specimens were idealized flexural specimens that can be interpreted as half a beam length in a rigid frame structure. The reversing transverse load applied at the end of the beam simulates the force at the inflection point of a beam in a frame carrying reversing lateral loads. The test specimen was anchored to a very substantial reinforced concrete base, oriented in a vertical position, and loaded at its upper end as shown in Figures 4.1 and 4.5a.

The large scale (prototype) specimen was constructed to approximately half full-size. The three small scale (model) specimens were 1/6 scale versions of the prototype. Details and dimensions of the specimens are shown in Figure 4.1.

Each specimen was reinforced longitudinally with three bars in each face. No. 6 bars (0.75 in. diameter) were used in the prototype, and 0.125 in. diameter bars in the models. The resulting reinforcing percentage is 1.22% in each face, based on the gross dimensions of the section. Shear reinforcement (designed to prevent any significant distress in shear) consists of #3 bar and D0.05 inch wire closed hoops for the prototype and the models, respectively. Nominal dimensions, reinforcing details and cross sections are shown in Figures 4.1(a), (b), and (c).

The base foundation was designed so that cracking would be minimal. This was accomplished by providing #10 bar for the prototype and D0.25 inch mechanically deformed wire for the models. In addition, the base foundation was externally post-tensioned to the supporting base with steel rods.

Materials used for the test specimens are summarized in Table 4.1. For the prototype specimen, the prototype concrete mix described in Chapter 2 was used, and #6 bars with mechanical properties as presented in Chapter 3 were used as longitudinal reinforcement. For all of the model specimens, Microconcrete III (presented in Chapter 2) was used. Since the main variable in this study was the type of deformation on the model reinforcement, three different types of model bar (with respect to degree of deformation on the surface of the bar) were provided as a model longitudinal reinforcement. The first specimen was reinforced with smooth round wires (called herein "specimen MR"). The second one used standard deformed model bars (specimen MS), and the third specimen was
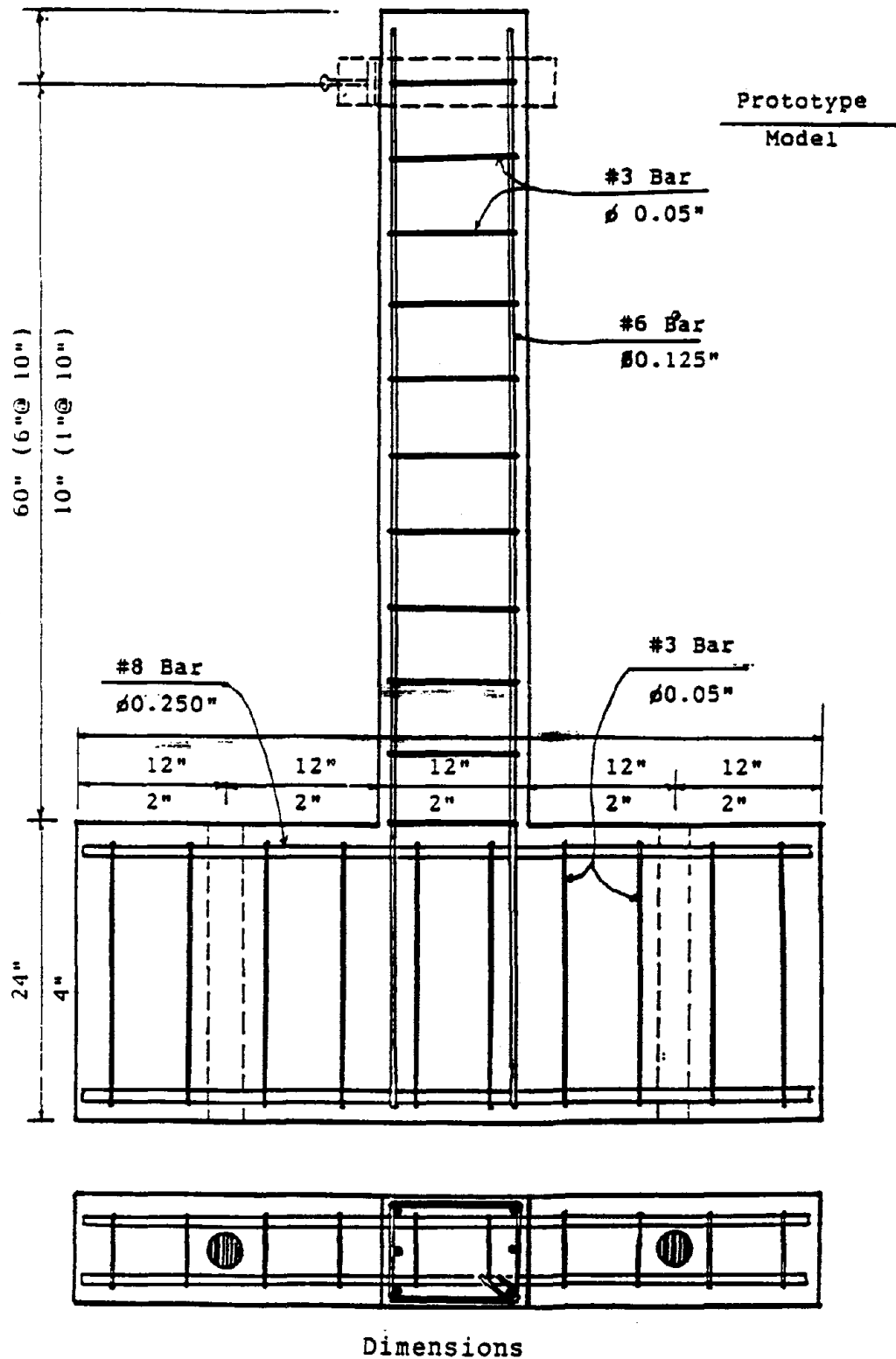
Figure 4.1. Reinforcement Layout.

4-3

#6 Bar

#3Bar

9"

1.5

1.5"

12"

(a) Prototype

See Table 4.1

⌀ 0.05"

1.5"

1/4"

1/4"

2"
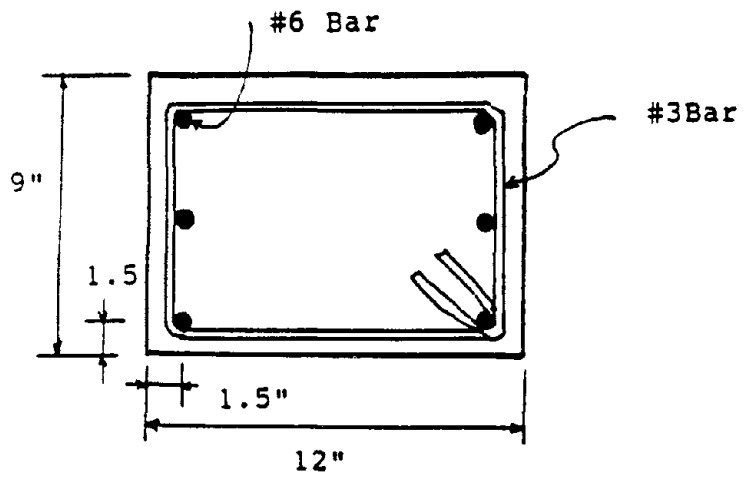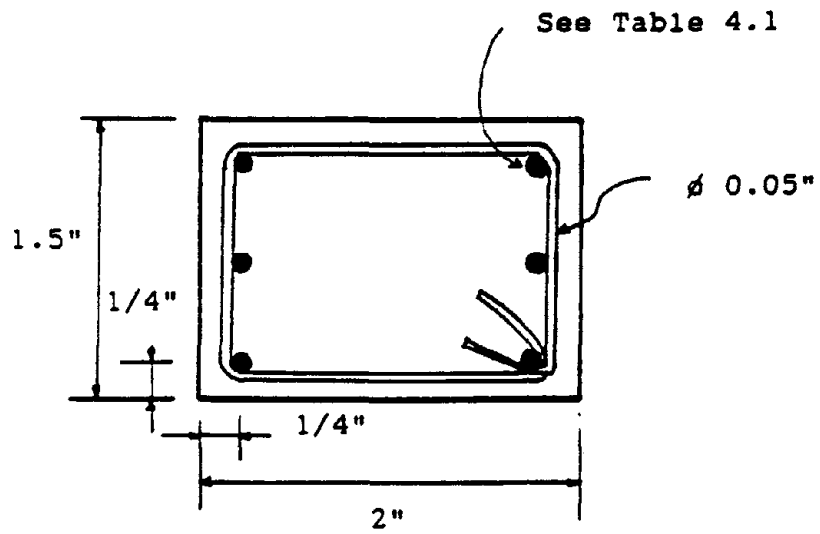
(b) 1/6 Scale Model

Fig. 4.2 Reinforcement Layout

Table 4.1  Materials Used for Specimens

| Specimen | Concrete | Longitudinal Reinforcement | | | | |
|---|---|---|---|---|---|---|
| | | Type | No. Used | $A_s$ (in$^2$) | $f_y$ (ksi) | $A_s f_y$ (kips) |
| Prototype | Prototype Concrete | #6 Bar | 6 | 2.64 | 66 | 174.2 |
| Model MR | Microconcrete III | Round Wire | 6 | 0.0678 | | |
| Model MS | Microconcrete III | Standard Deformed | 6 | 0.0630 | 78 | 4.9 |
| Model MT | Microconcrete III | Thread (Small) | 2 | 0.0158 | 62 | 4.9 |
| | | Thread (Large) | 4 | 0.0556 | 71 | |

reinforced with threaded rods (specimen MT). The mechanical properties of the reinforcement are given in Chapter 3.

### 4.2.3 Specimen Preparation

The specimens were cast in forms constructed of 3/4 inch structural grade plywood. The reinforcing bars were assembled with stirrups to form a rigid cage using wire ties. The reinforcing cage was secured in the form using steel chairs and the holes on the form to maintain exact positioning.

All specimens were cast in a horizontal position. The mix was placed in two equal depth layers. Each layer was uniformally compacted with an electric internal vibrator. After casting, the specimens were covered with plastic sheet. The forms were removed one day after casting; the prototype specimen was kept moist with plastic cover, while the model specimens were soaked into water until testing. The specimens were tested about two weeks after casting.

### 4.2.4 Test Apparatus

The function of the test apparatus was to transfer the reversing lateral force from the actuator to the top of the column specimen, measure the load, and measure the deflection at the top of the column and the rotation at the bottom of the beam.

Prototype Test ----- Figure 4.3 shows the outline of the prototype beam test frame. The specimen base was fixed against translation and rotation by anchoring it to the structural steel test frame with high strength steel rods. A load reaction bracket in the form of a triangle was built on the strong base girder. A 55 kip capacity hydraulic actuator was mounted on the shelf which was welded to the vertical member of the reaction bracket. Figure 4.5(a) is a photo of the test apparatus with the specimen on it.

Model Test ----- Figures 4.4 and 4.5(b) shows the model column test apparatus. An existing model testing table made of grid type steel bridge decking was used. Two small angle brackets were brackets were bolted to the table; one was for a 2.2 kips MTS actuator, and the other was for supporting the model specimen. The base foundation of the model specimen was fixed against translation and rotation by bolting it to the bracket. A photo of the model test apparatus is shown in Figure 4.5(b).

55 kips
MTS Actuator

Prototype
Specimen

1 3/8" High
Strength Bolts

Load
Cell

2 L4x4

2 W8x21

2 W8x21

2 W14x16
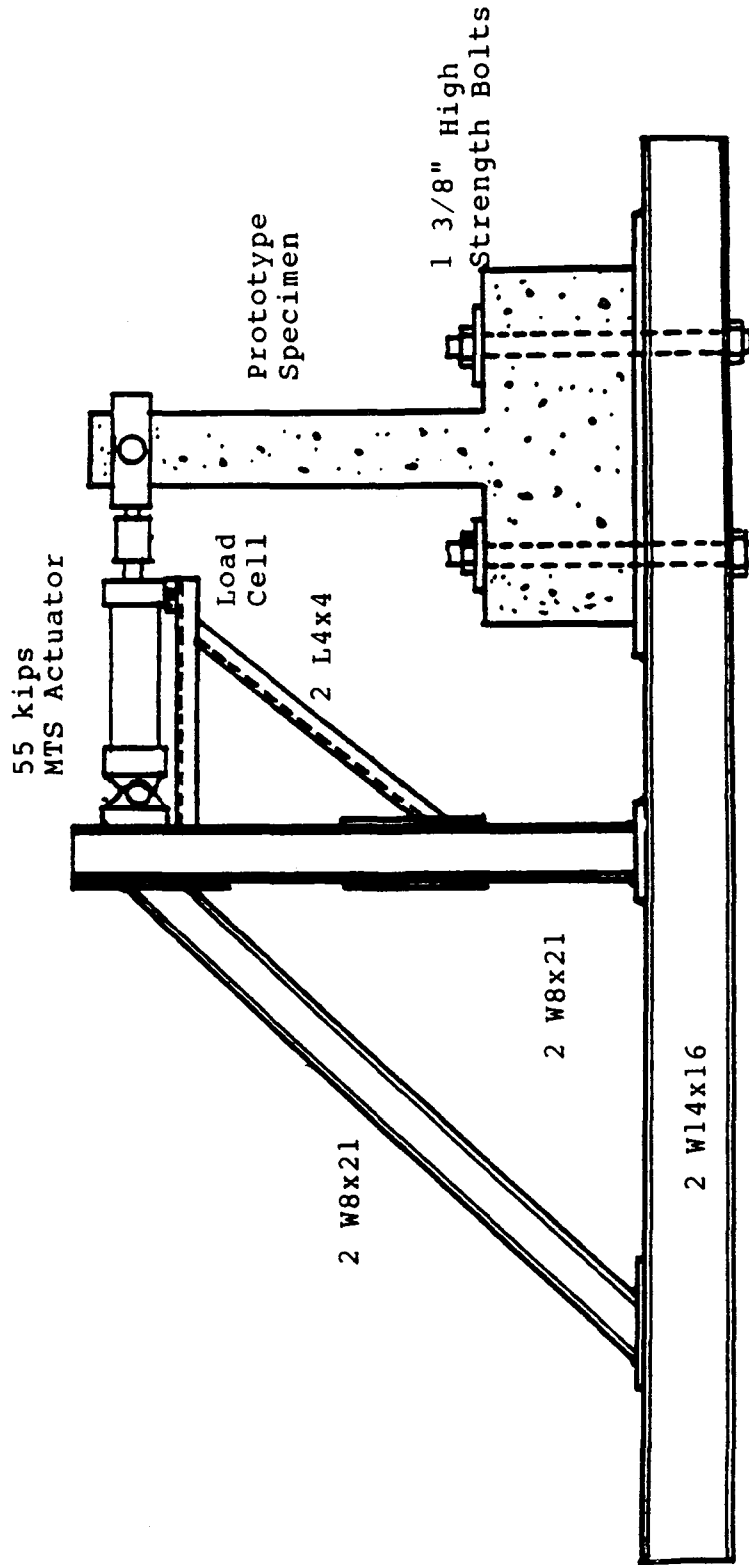
Figure 4.3. Prototype Beam Test Frame.

4-7
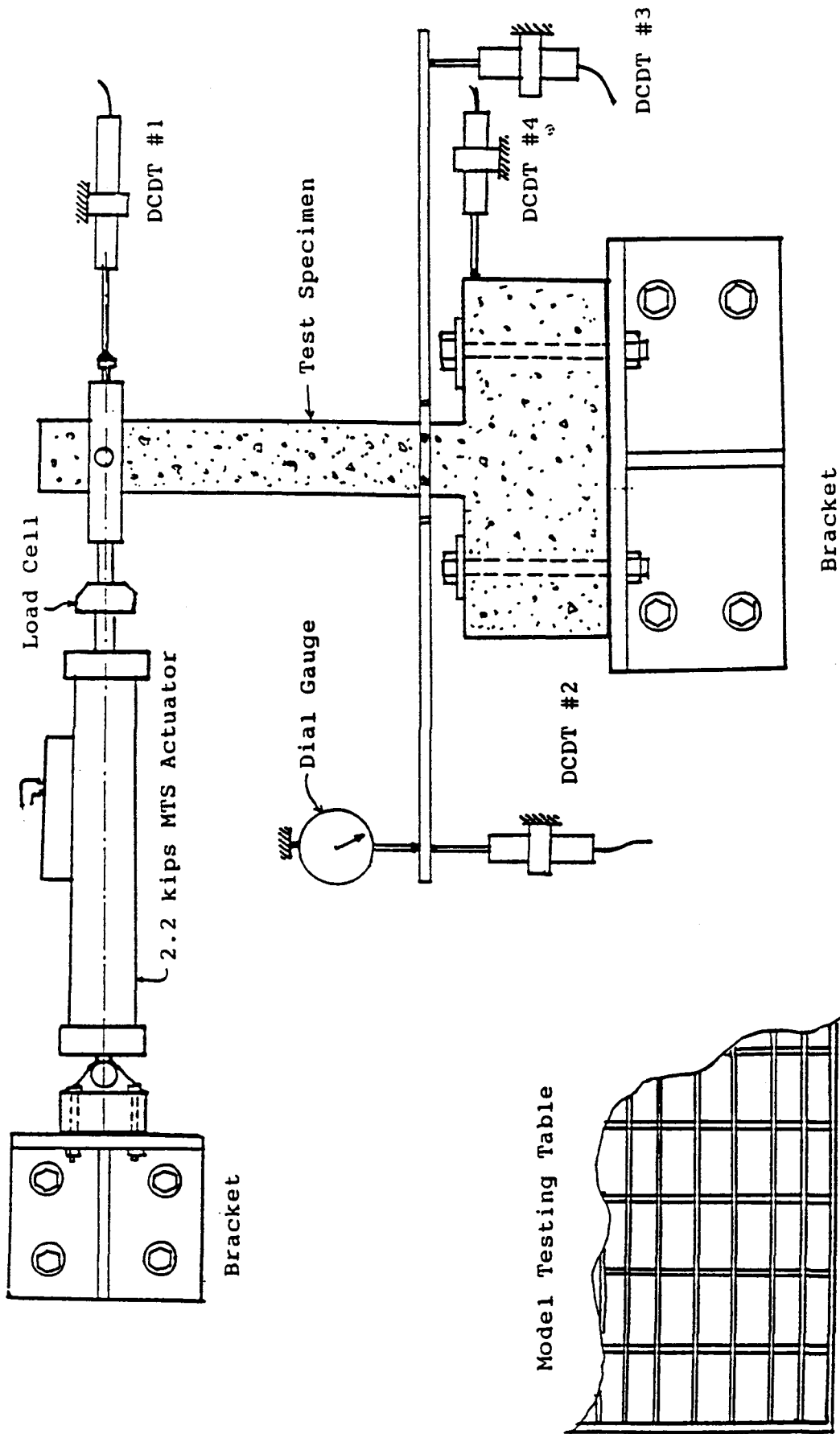
Fig. 4.4  Model Column Test Setup
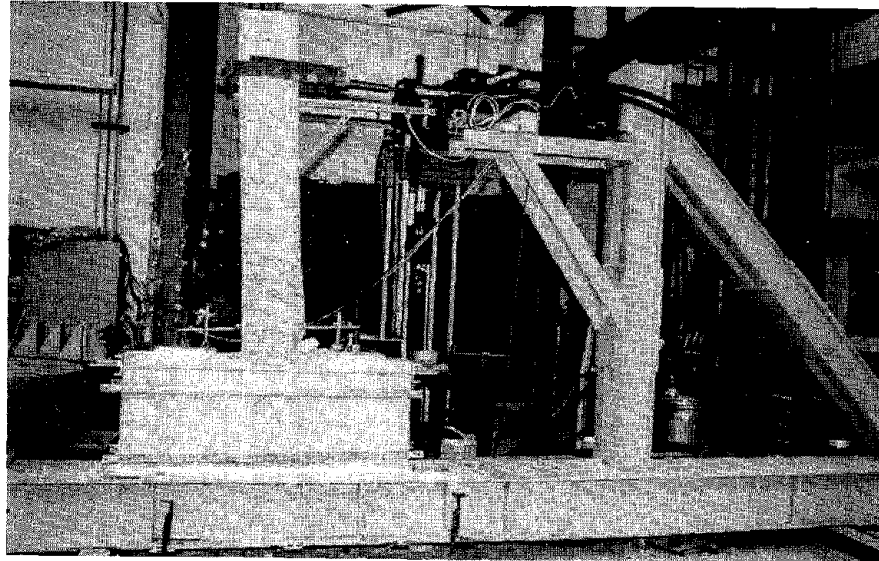
(a) Prototype.
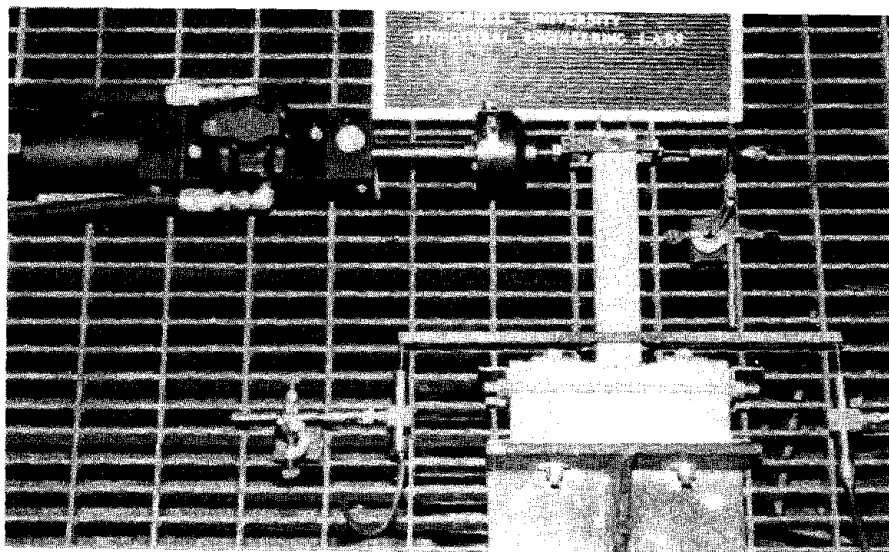


(b) Model.

Figure 4.5. Test Setup.

4-9

One of the most important devices in both the model and prototype test set-ups was a load transferring device from the actuator to the center of the test specimen section. The cyclic load transfer device is shown in Figure 4.6. It was made of heavy steel plates welded in the form of a box with pin-connected rotating arms. The specimen was tightened and aligned to center by turning two bolts. The rotating arms were connected to the actuator with a single bolt. The mechanism of the device was identical in both the model and the prototype tests.

### 4.2.5 Instrumentation

Three parameters were measured for each specimen: applied load, displacement at the top of the column, and rotation at the base of the column. For loading, a hydraulic, servo-controlled MTS structural test system with integral load cell was used. A 55 kips capacity actuator was used for the prototype test, while a 2.2 kips capacity actuator was used for the model tests. The top deflection was measured with a DCDT. With the use of the HP-data acquisition system, it was possible to measure the deflection to an accuracy of ± 0.00002 inches.

Since considerable damage was expected at the bottom of the column, the base rotation was measured at a distance equal to a half of the effective depth above the base foundation. At this point, a steel bar was attached to all four sides of the section by turning the screws as shown in Figure 4.7. DCDTs were mounted to both ends of the steel bar with magnetic supports. Mechanical dial gages were used alongside the DCDTs to check the electronic measurements.

The entire test was controlled by a HP-9825B calculator, and monitored with a HP 3052A Data Acquisition System. The load, displacement, and rotation were continually monitored and printed, and were also plotted on the calculator screen.

### 4.2.6 Test Procedure

Reversing cyclic loads were applied in a displacement controlled mode. The displacement at the top of the column was programmed to linearly increase and decrease in accordance with the pre-determined displacement history shown in Figure 4.8. It consisted of five levels; $0.5D_y$, $2D_y$, $4D_y$, and $6D_y$ in which $D_y$ was the theoretically calculated deflection at the top of the member when the reinforcement at the maximum moment section reached yield. Each load level had five cycles. The time required for each cycle was about 8 minutes; thus, the
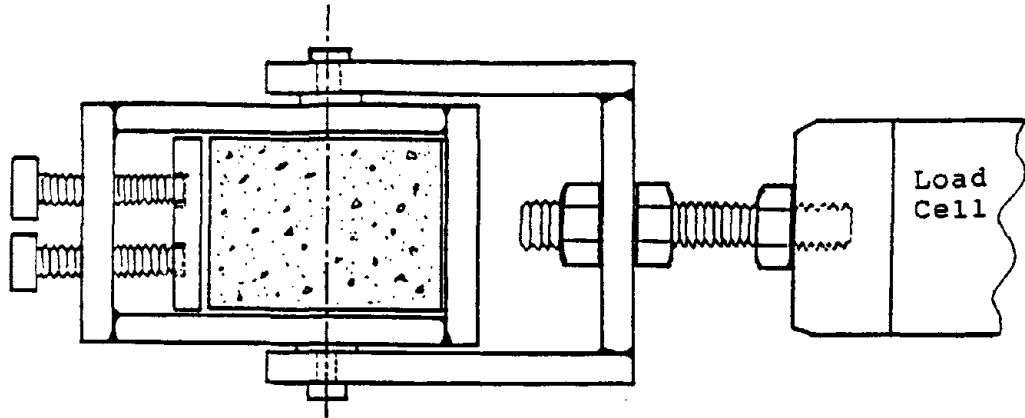
Fig 4.6 Cyclic Load Transfer  Device.
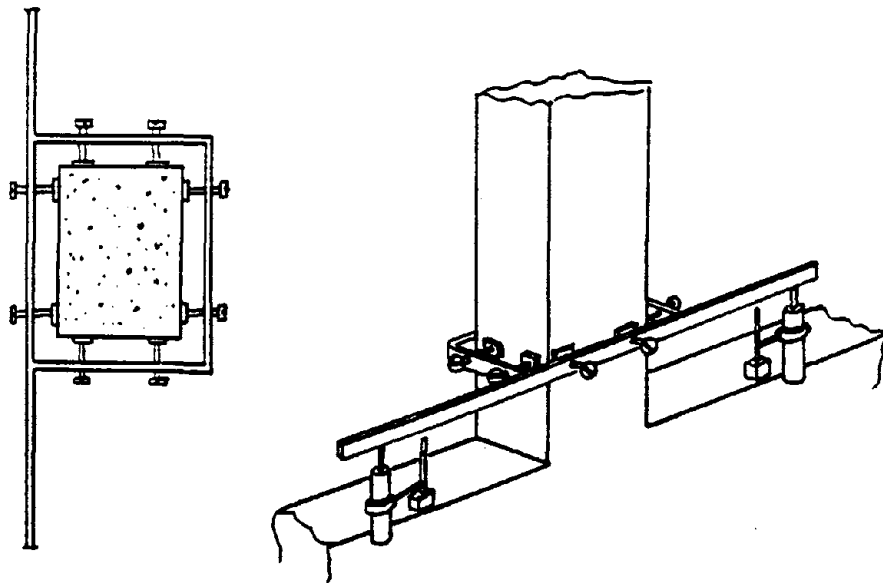
Fig. 4.7  End Rotation Measurement Device
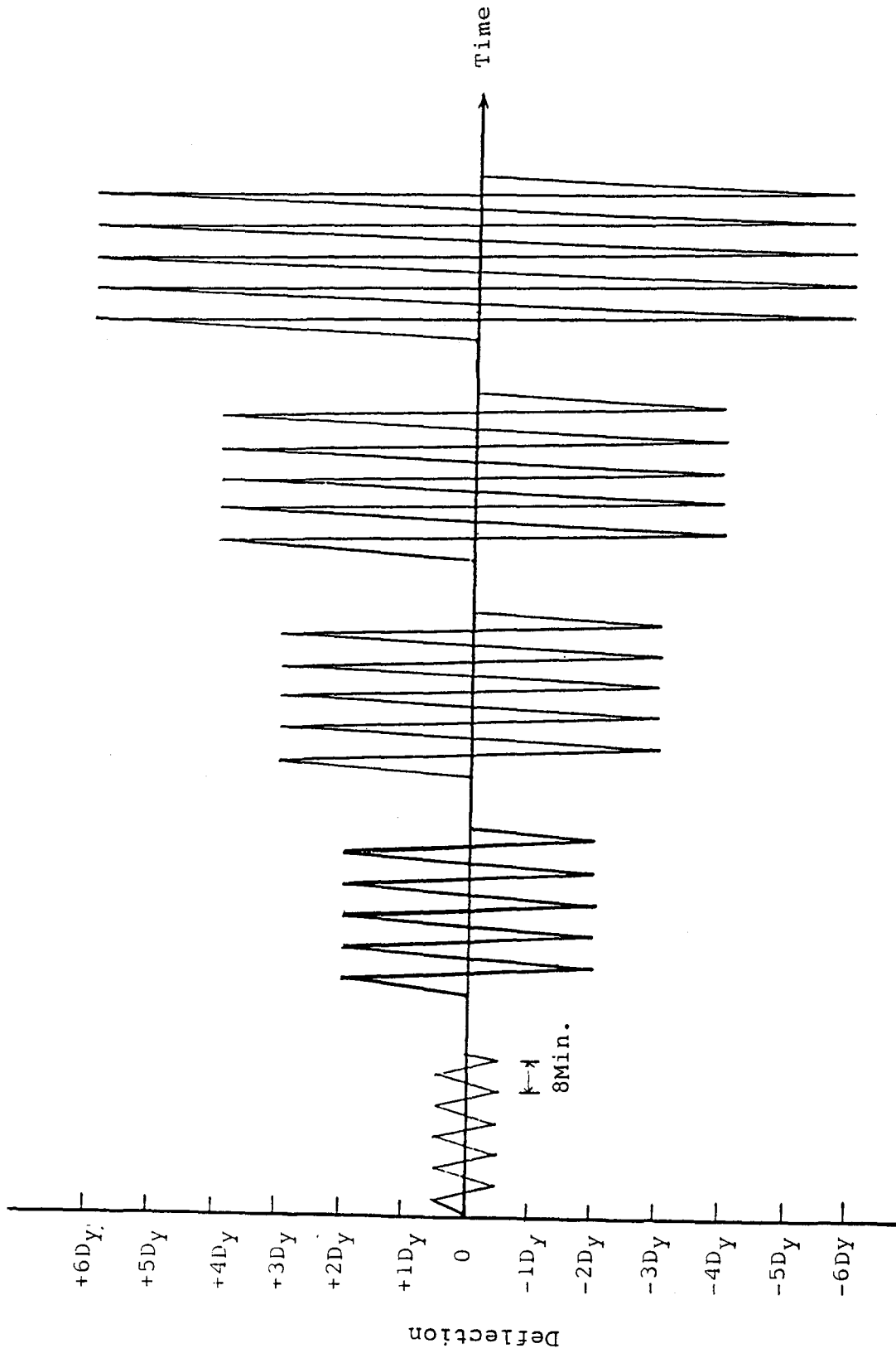
Fig. 4.8 Displacement History

loading rate was increased as the amplitude became larger. After finishing each set of 5 cycles, the bolt of the load transferring device from the actuator to the specimen was loosened in order to release any residual forces or stresses in the member. Then the bolt was tightened again for next load level. Throughout each test, the load-displacement relation was monitored continuously on the computer screen. Data points for all test parameters were taken intermittently to produce a smooth curve. Dial gauge readings were taken at every data point for the first few cycles to insure proper operation of the electronic instruments.

Crack patterns were monitored carefully throughout the test and marked on the specimen. In this way a complete cracking history was documented.

## 4.3. Test Results

### 4.3.1. Cracking Behavior

Figure 4.9 shows the cracking patterns for the prototype specimen along with the model specimens at all considered loading levels.

At a ductility factor of 0.5 (Figure 4.9a), six approximately equally spaced cracks were developed in each face of the prototype specimen. These cracks extended over approximately half the beam length. A similar cracking pattern, but with fewer cracks and slightly larger scaled spacing, was observed in the threaded rods model at this loading level. The number of cracks observed in the standard deformed bars specimen was less than that of the threaded rods specimen at this stage, and only a single main crack was observed at the bottom of the plain bars specimen.

At a ductility factor of 2.0, a large number of deep, closely spaced cracks was developed in both the prototype and the threaded bars specimen. Cracking in the standard deformed bars specimen was quite similar to that in the threaded bars specimen. The plain bars specimen failed at with one major crack at the bottom of the beam.

Significant damage at the bottom of the standard deformed bars specimen was observed at a ductility factor of 3.0. The threaded bars specimen cracking pattern was similar to that of the prototype but with fewer cracks.
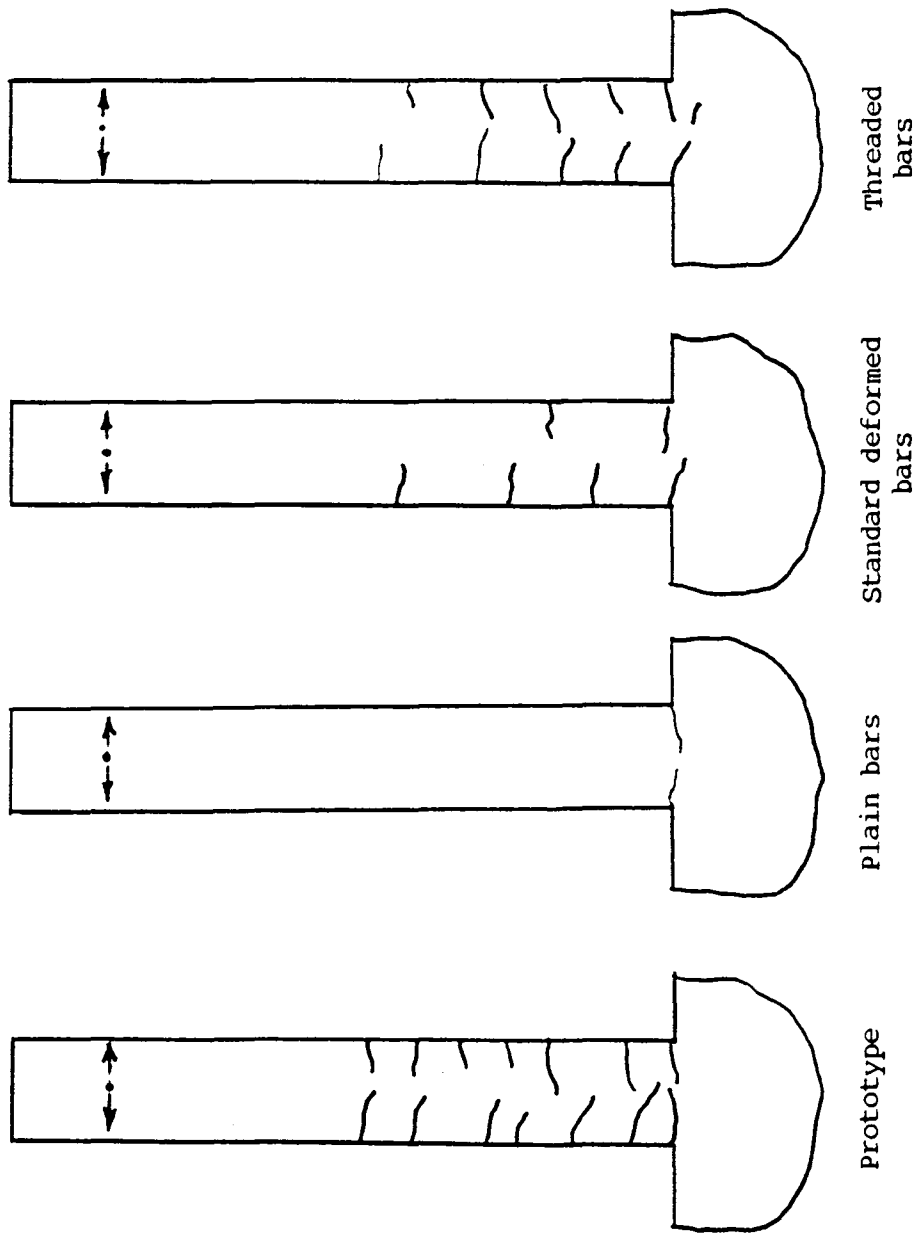
Figure 4.9.a. Cracking Patterns at a Ductility Factor of 0.5 .

Threaded bars

Standard deformed bars

Plain bars
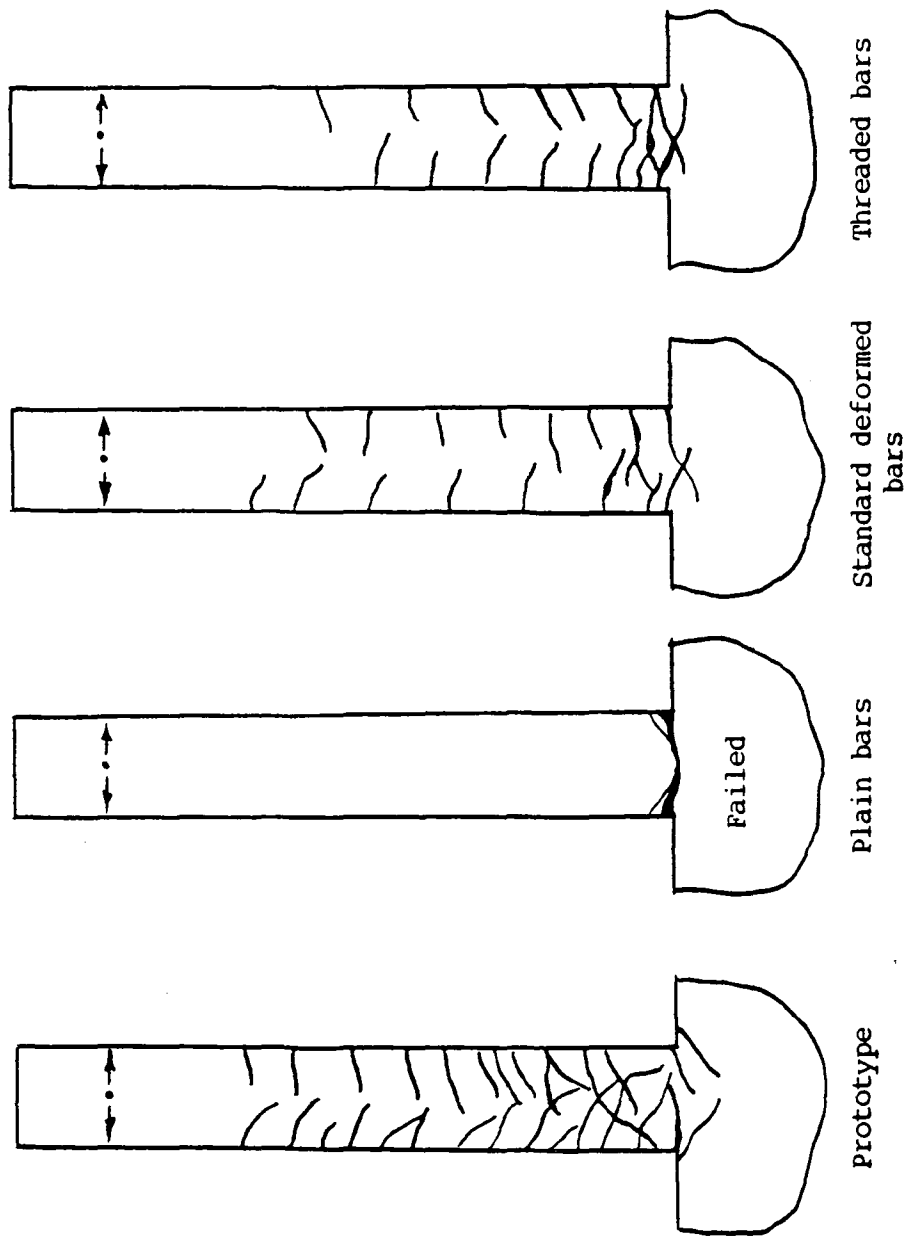
Prototype

Figure 4.9.b. Cracking Patterns at a Ductility Factor of 2.0 .

Threaded bars

Standard deformed bars

Plain bars
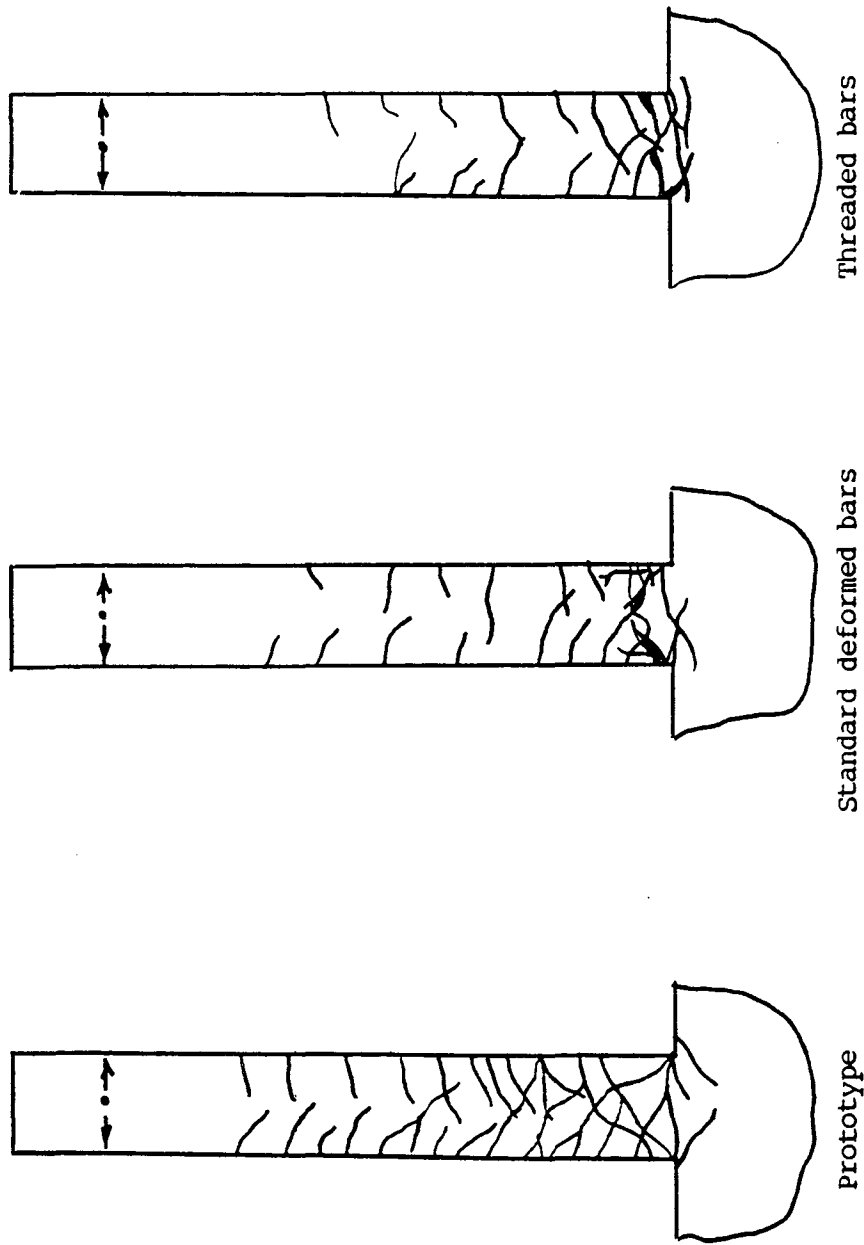
Failed

Prototype

Figure 4.9.c. Cracking Patterns at a Ductility Factor of 3.0 .

Prototype

Standard deformed bars

Threaded bars

Prototype          Standard deformed bars          Threaded bars

Failed.

Figure 4.9.d. Cracking Patterns at a Ductility Factor of 4.0 .
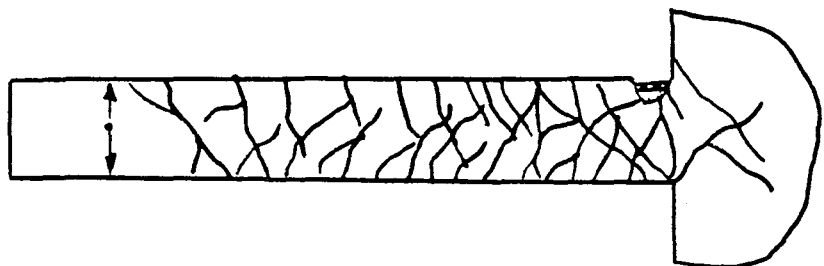
Figure 4.9.e. Cracking Patterns at a Ductility Factor of 6.0 .

The standard deformed bars specimen failed at a ductility factor of 4.0 due to excessive damage at the bottom. Also, at this load level, cracks extended almost to the top of the prototype specimen. The overall behavior and cracking response of the threaded bars specimen was still closer to that of the prototype than the standard deformed bars specimen.

At the final stage (ductility factor = 6.0), the threaded bars specimen cracking pattern was close to that of the prototype although substantially fewer cracks were observed.

In summary, the threaded bars model specimen cracking behavior showed the best correlation with the prototype behavior through the different stages of loading. This can be directly attributed to the better representation of bond characteristics with this type of highly deformed model reinforcement.

### 4.3.2. Hysteresis Response

#### 4.3.2.1 Load-Displacement Response

The hysteretic load-displacement response was of primary importance in this study since it gives an overall basis for evaluating the model response, including degradation rates and energy absorption, and with less emphasis on local response characteristics such as cracking and bond-slip.

Figures 4.10 through 4.13 represent the load-displacement hysteresis loops for the different models at ductility factors of 2.0, 3.0, 4.0, and 6.0 respectively. The model responses were scaled up to prototype size by using the appropriate scaling factors as follows:

$$(Displacement)_p = (Displacement)_m \times s_\ell$$

$$(Force)_p = (Force)_m \times s_\ell^2$$

This facilitated the plotting of both the prototype and model responses on the same set of axes for direct comparison.

At a ductility factor of 2.0, the plain bars specimen failed by excessive bond slip as shown in Figure 4.10.a. The standard deformed bars specimen showed fair agreement with the prototype response at this load level (Figure 4.10.b). Essentially perfect agreement between the threaded bars model and the prototype was recorded. (Figure 4.10.c).
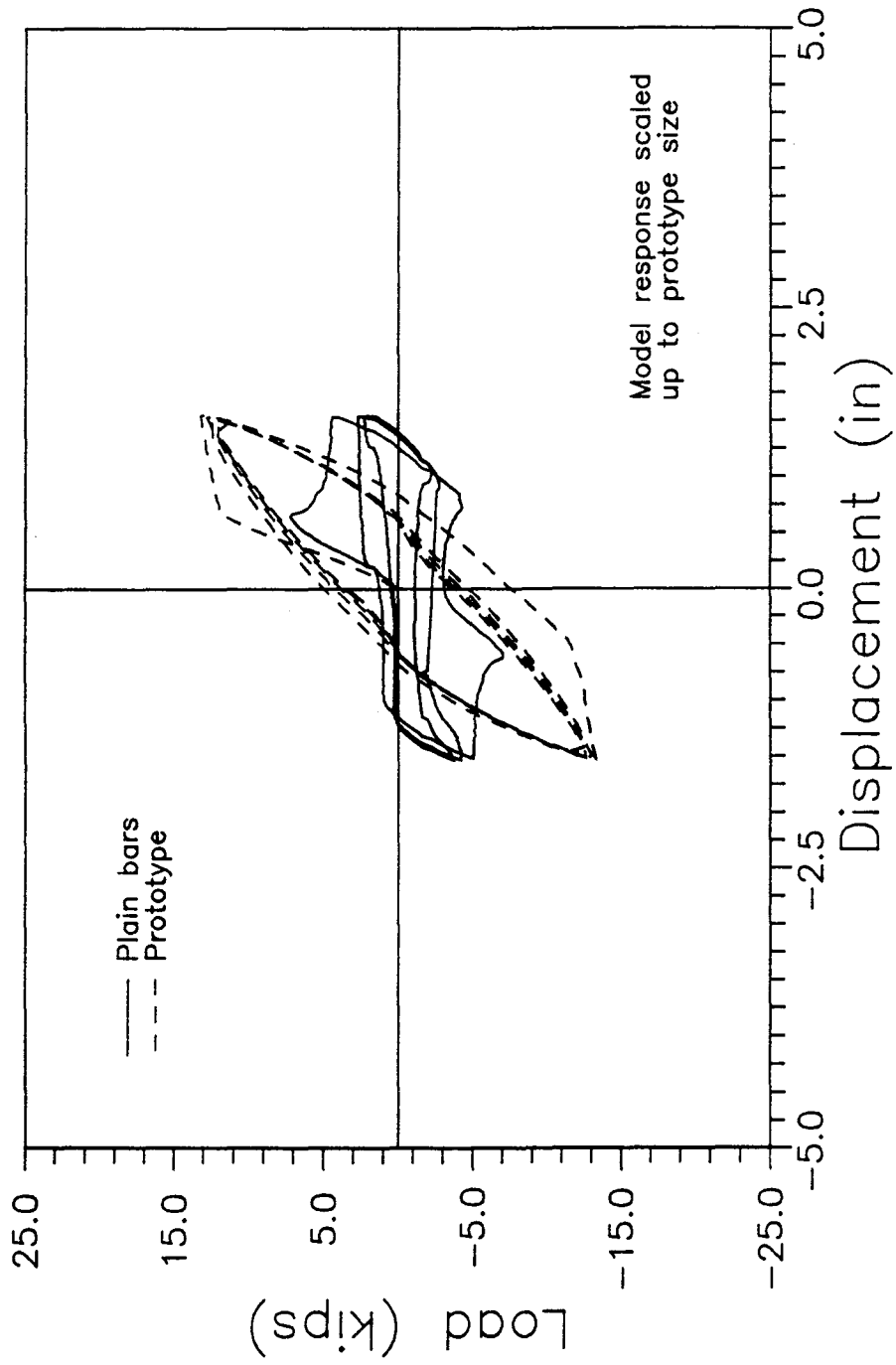
Figure 4.10.a. Plain Bar Versus Prototype Response at a Ductility Factor of 2.
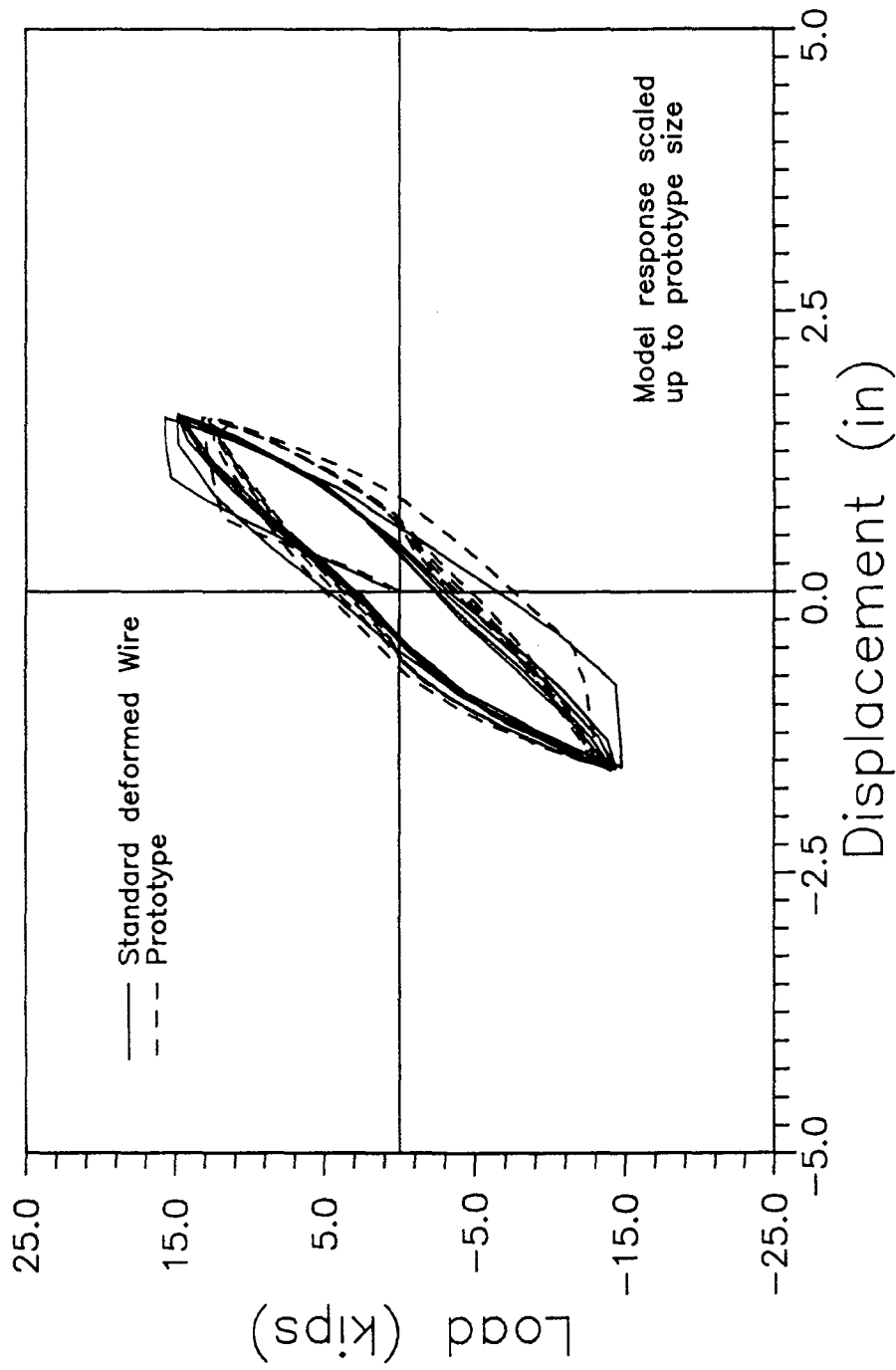
Figure 4.10.b. Standard Deformed Wire Versus Prototype
Response at a Ductility Factor of 2.
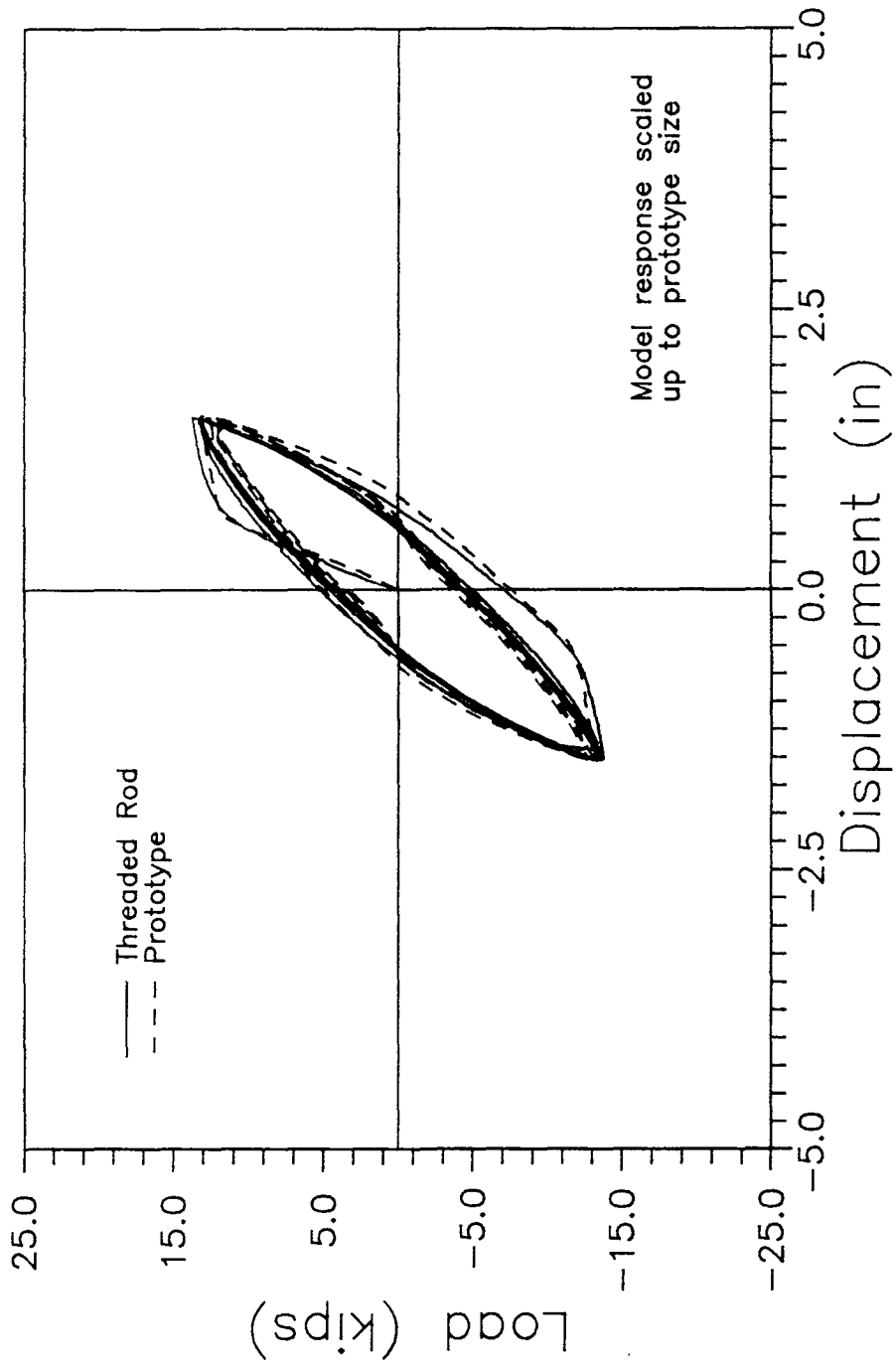
Figure 4.10.c. Threaded Rod Versus Prototype Response
at a Ductility Factor of 2.

At a ductility factor of 3.0, the prototype specimen hysteretic response loops showed some pinching due to the opening and closing of cracks. The hysteresis loops were fairly stable, and showed very little reduction of strength with cycling. The standard deformed bars specimen showed fair agreement with the prototype response. Some pinching was reproduced at the model level at this stage, but not as much as that observed in the prototype. It was also observed that the model specimen strength was gradually decreasing with cycling. (Figure 4.11.a).

The threaded bars specimen response at a ductility factor of 3.0 is shown in Figure 4.11.b. The hysteresis loops were stable with cycling, showing no reduction in strength. No pinching in the hysteresis loops was observed. This can be explained as a result of the lack of sufficient bond-slip in the threaded bars specimen, which consequently reduced the cracks widths and the pinching phenomena.

At a ductility factor of 4.0, the hysteresis loops of the prototype specimen showed more pinching but were fairly stable with cycling. This behavior was not reproduced in the standard deformed bars specimen which showed a significant reduction in strength with cycling. At the end of the 5th cycle at a ductility factor of 4.0, the strength of the standard deformed bars specimen was only about half its original strength (Figure 4.12.a).

The threaded bars specimen response (Figure 4.12.b.) was still stable with cycling at ductility factor 4.0, but very little pinching was recorded. The strength values on both sides of the hysteresis loops were in good agreement with those of the prototype.

At a ductility factor of 6.0, both the prototype and the threaded bars model showed strength reduction with cycling. Furthermore, more pinching was reproduced at model scale (Figure 4.13).

It can be seen from the previous discussion that the use of threaded bars as model reinforcement gives the best correlation with the prototype response at a ductility factor of 6. The lack of sufficient pinching will lead to more (scaled) energy absorption in the model than in the prototype.
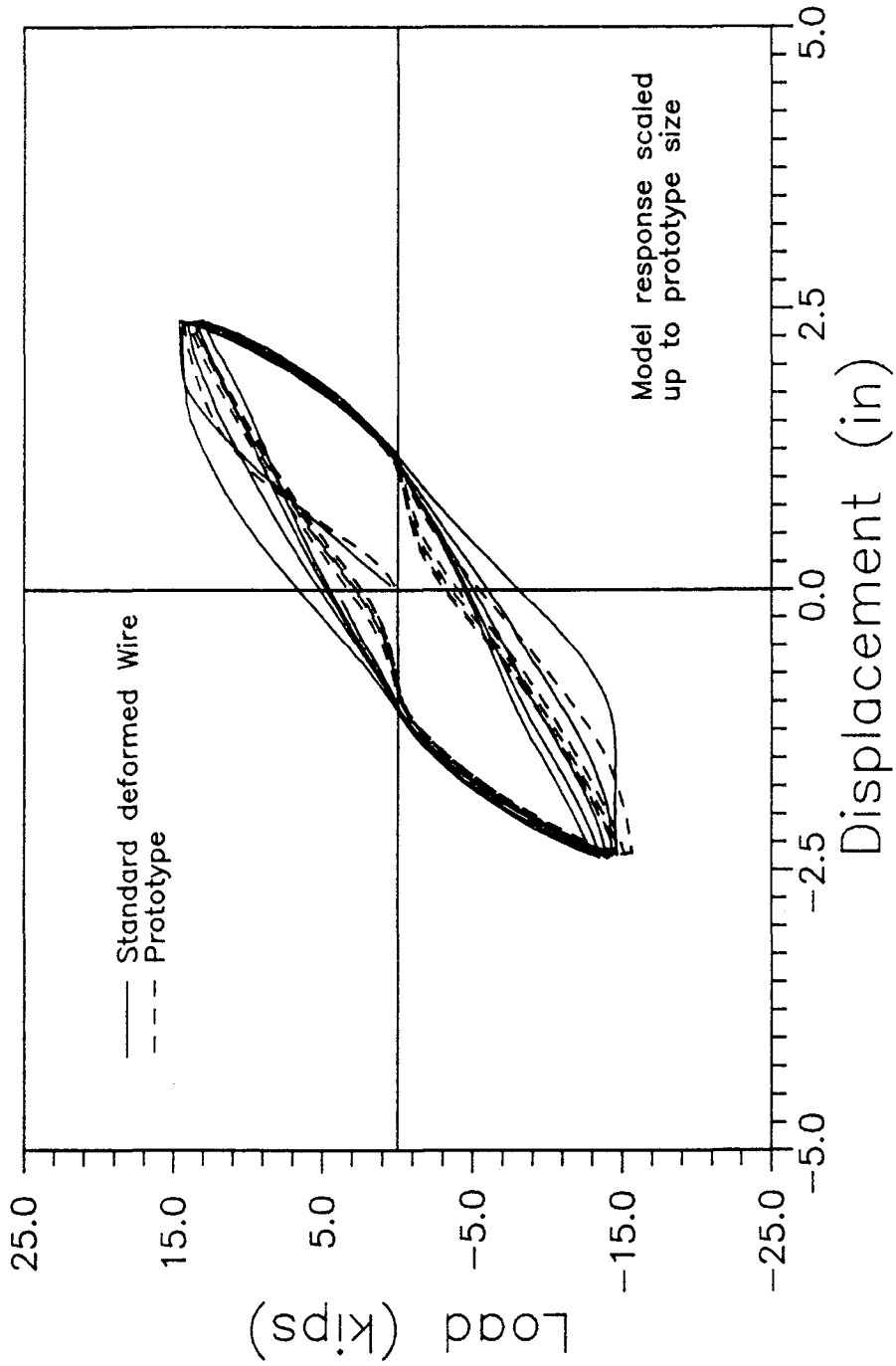
Figure 4.11.a. Standard Deformed Bar Versus Prototype Response at a Ductiliyt Factor of 3.
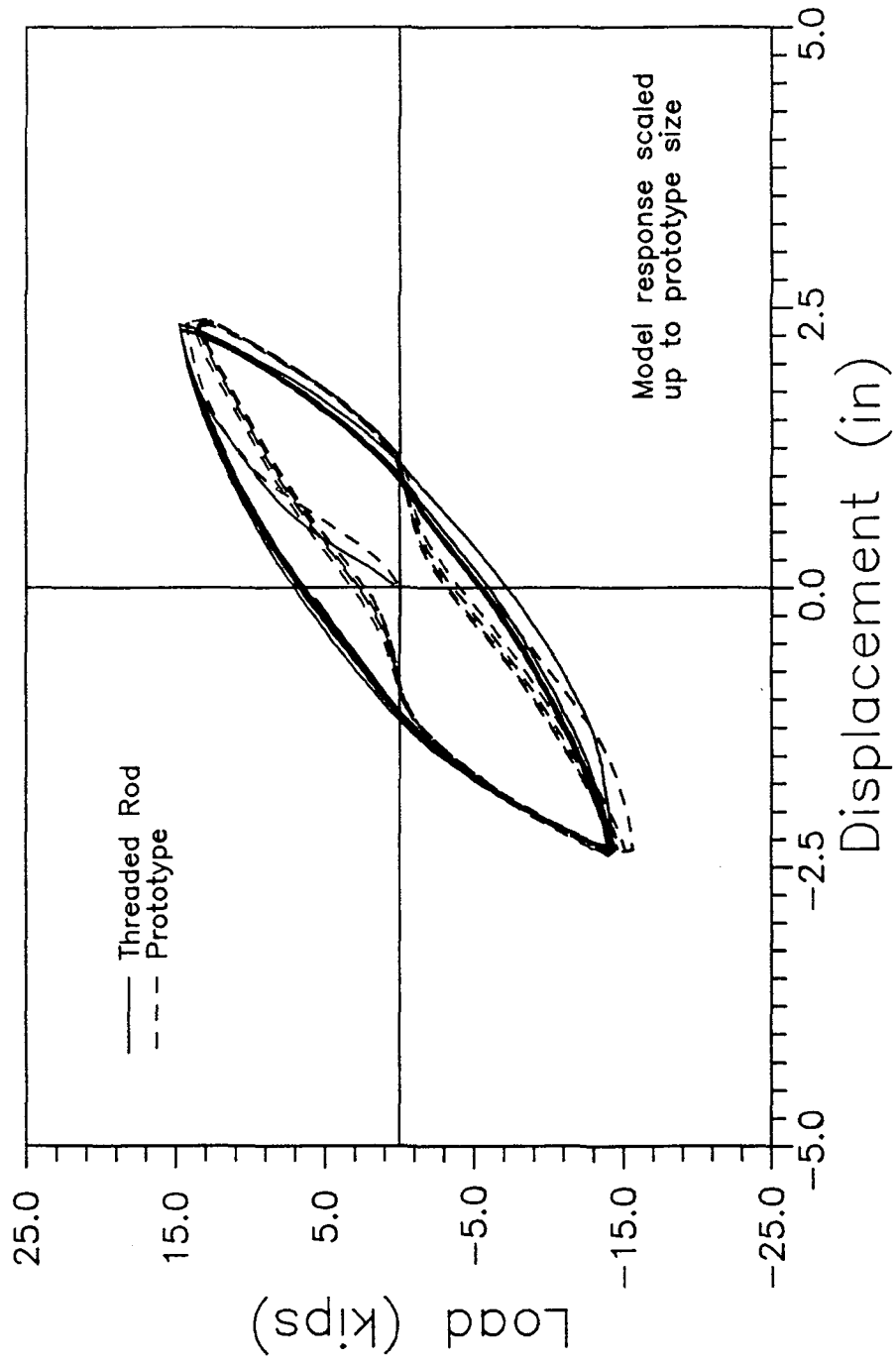
Figure 4.11.b. Threaded Rod Versus Prototype Response
at a Ductility Factor of 3.
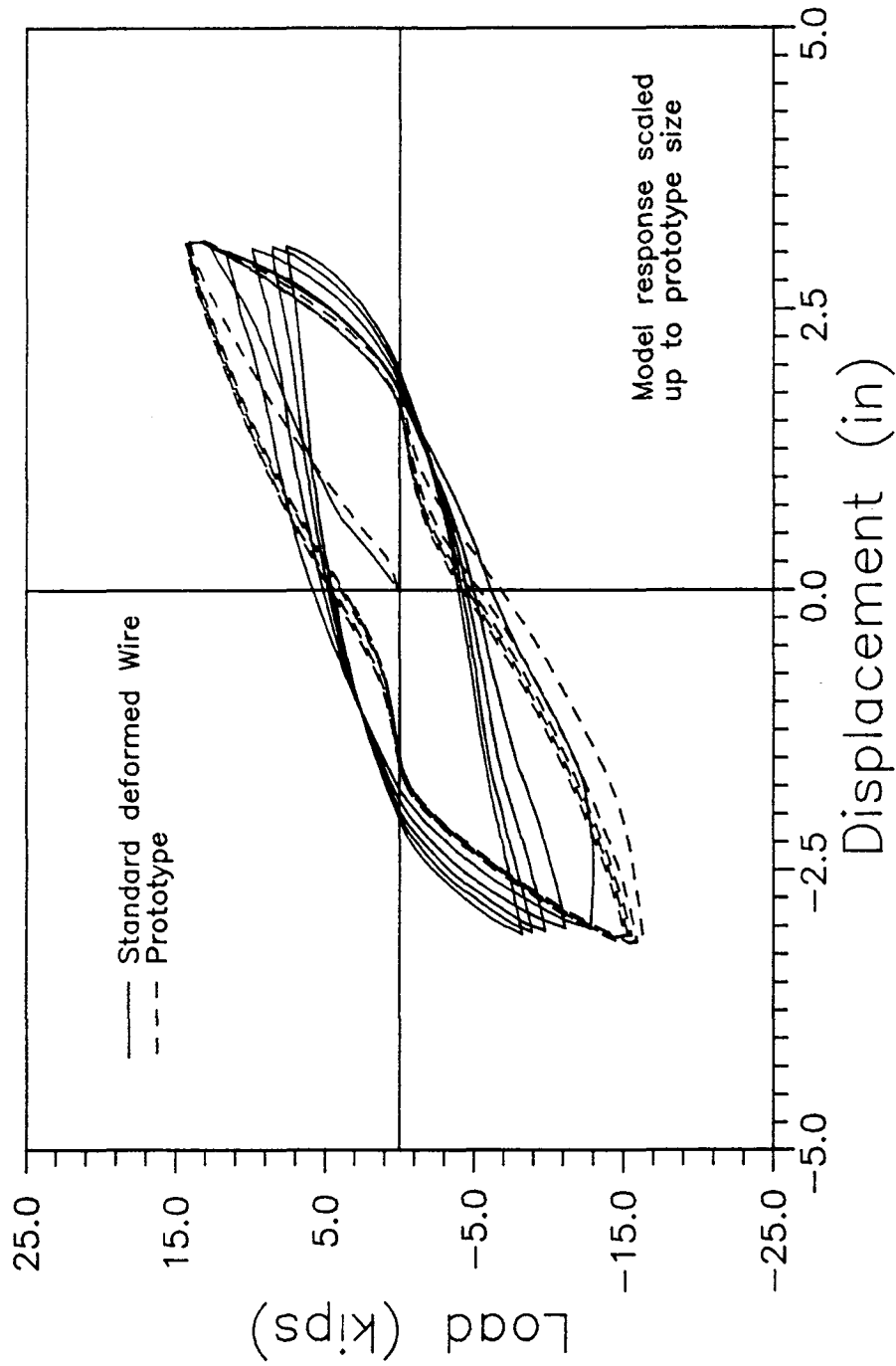
Figure 4.12.a. Standard Deformed Wire Versus Prototype
Response at a Ductility Factor of 4.
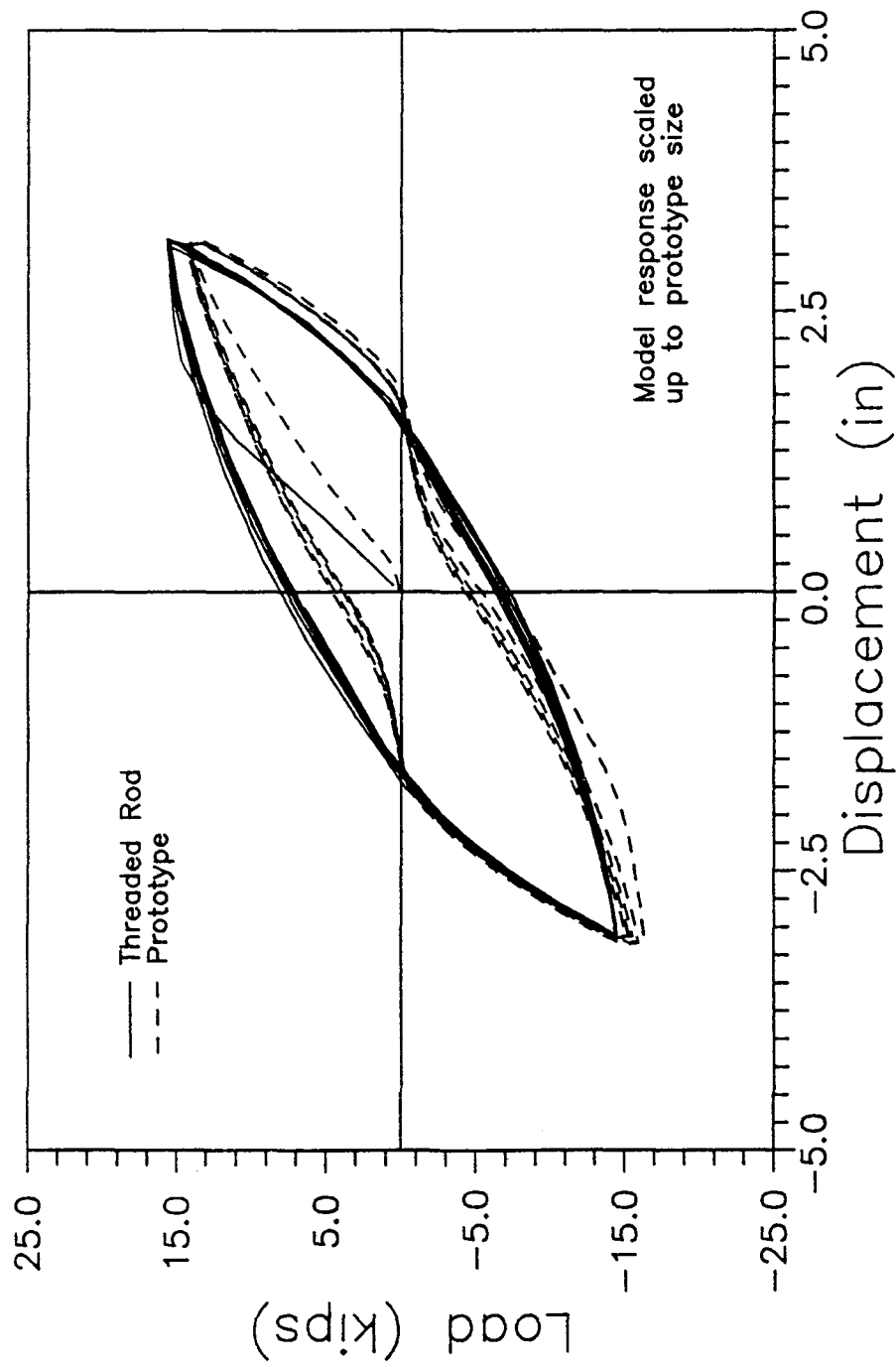
Figure 4.12.b Threaded Rod Versus Prototype Response at a Ductility Factor of 4.
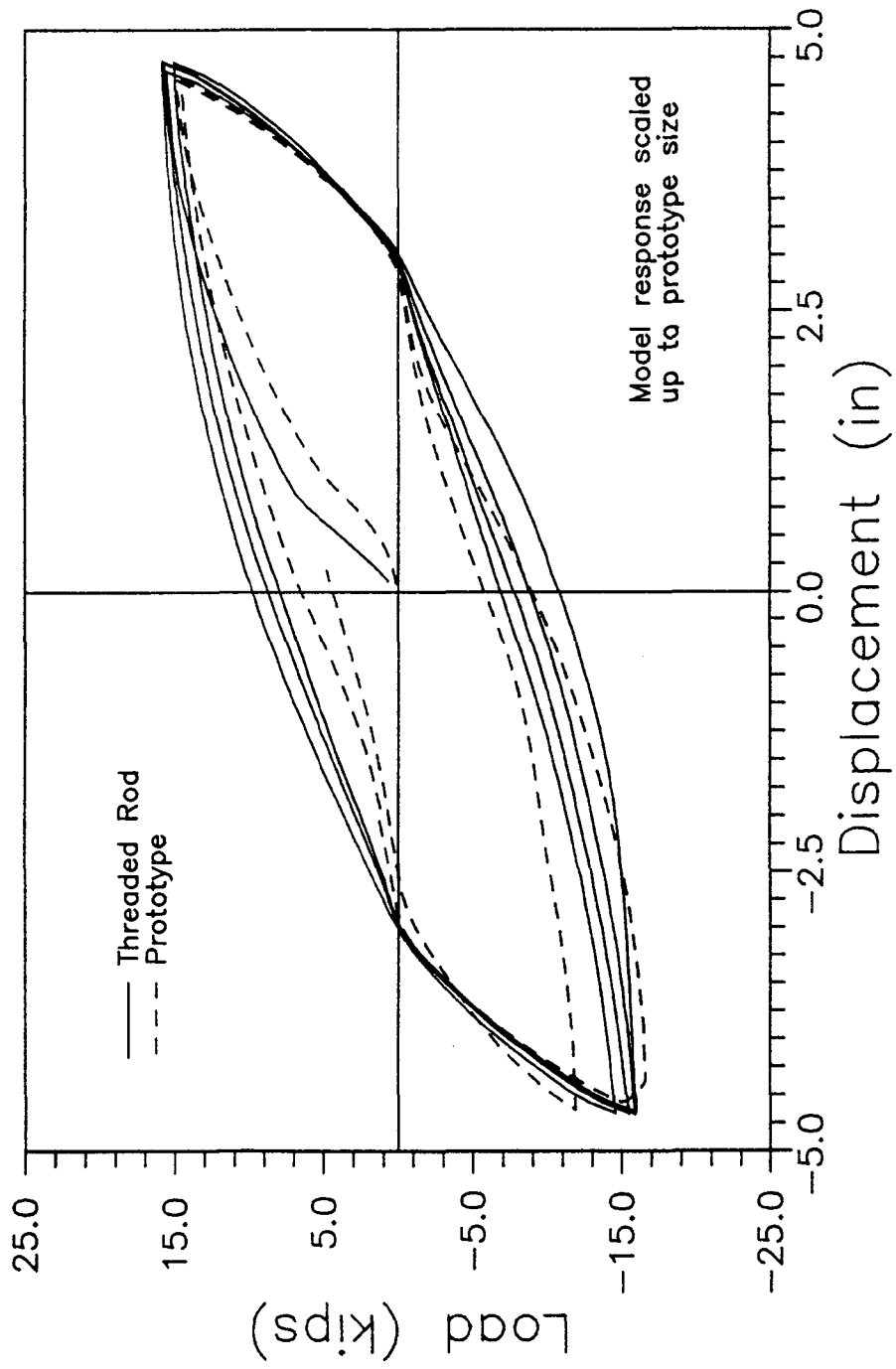
Figure 4.13. Threaded Rod Versus Prototype Response at a Ductility Factor of 6.

4-28

## 4.3.2.2. Moment-Rotation Response

The moment-rotation responses of the standard deformed bars, threaded bars, and the prototype specimens are introduced and discussed in this section. Results are shown in Figures 4.14 through 4.16. The essence of this comparison is to investigate the local behavior of the model and the contribution of cracking and bond slip on the model response.

The response of the models was again scaled to the prototype size using the appropriate scaling factors as follows:

$$(\text{Rotation})_p = (\text{Rotation})_m$$

$$(\text{Moment})_p = (\text{Moment})_m \times s_\ell^3$$

At a ductility factor of 3.0, the standard deformed bars specimen moment-rotation response was in fair agreement with that of the prototype (Figure 4.14a). The model rotation was generally higher than the prototype rotation. This can be explained as a result of the fewer number of cracks developed in the model, which suggests that a significant part of the inelastic beam rotation will take place at the lower cracks. The rest of the beam can be almost rotating as a rigid body about the lower sections (up to t/2 in this case).

On the other hand, because of the better crack distribution in the threaded bars model, the inelastic beam rotation will take place over a larger number of cracks. The spread of the inelastic beam rotation over a longer distance of the beam length resulted in the better agreement between the model and prototype moment-rotation responses shown in Figure 4.14.b.

At a ductility factor of 4.0, the standard deformed bars specimen showed excessive local rotations and almost failed at the end of the 5th cycle (Figure 4.15.a).

Both the prototype and the threaded bars specimen hysteresis moment-rotation responses were stable with cycling. The prototype showed more pinching behavior than the model due to cracking and bond-slip, as shown in Figure 4.15.b.

At a ductility factor of 6.0, agreement between the threaded bars model and the prototype was quite good (Figure 4.16). The model hysteresis loops showed more pinching at this stage.
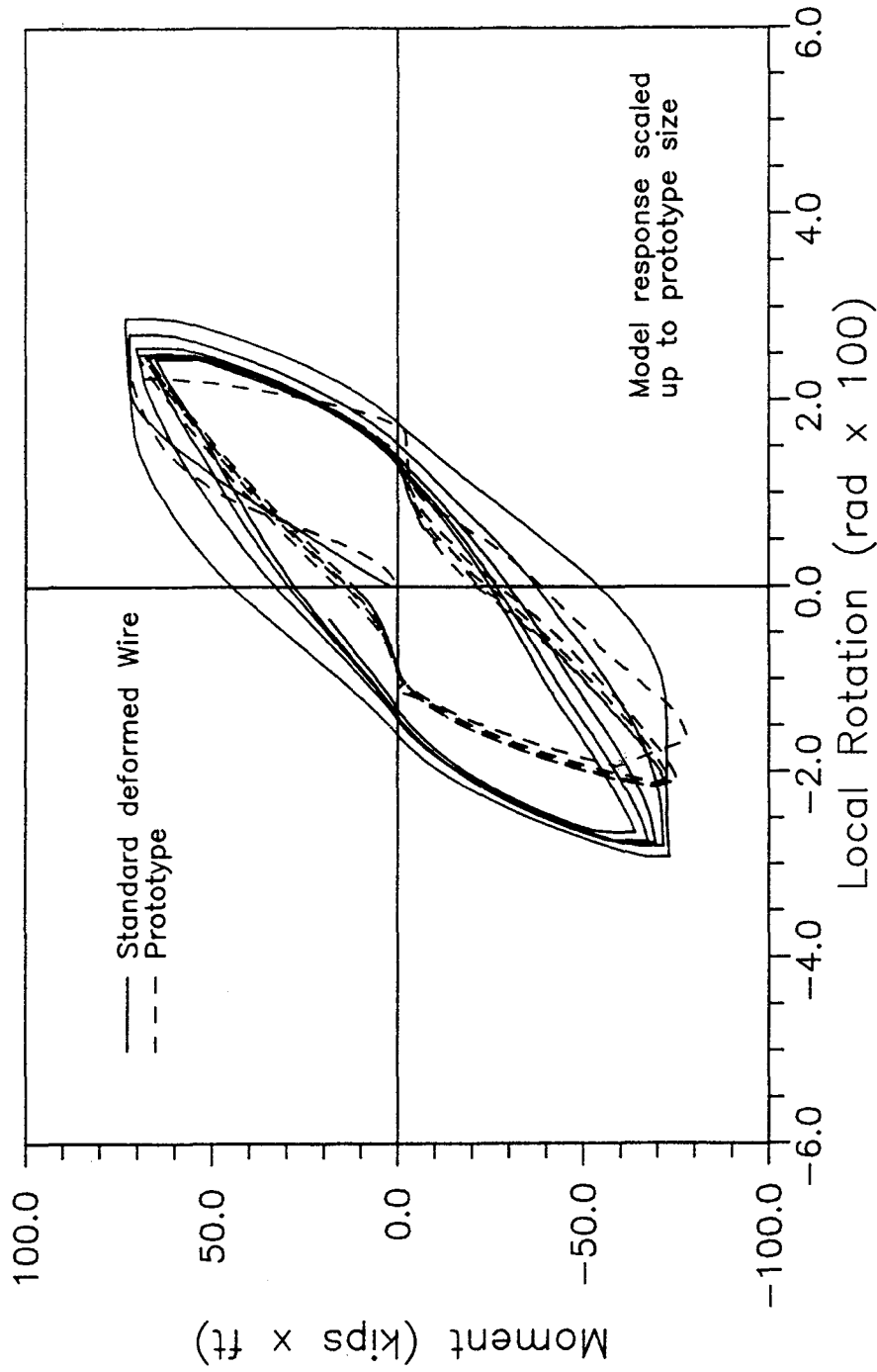
Figure 4.14.a. Standard Deformed Wire Versus Prototype Response at a Ductility Factor of 3.
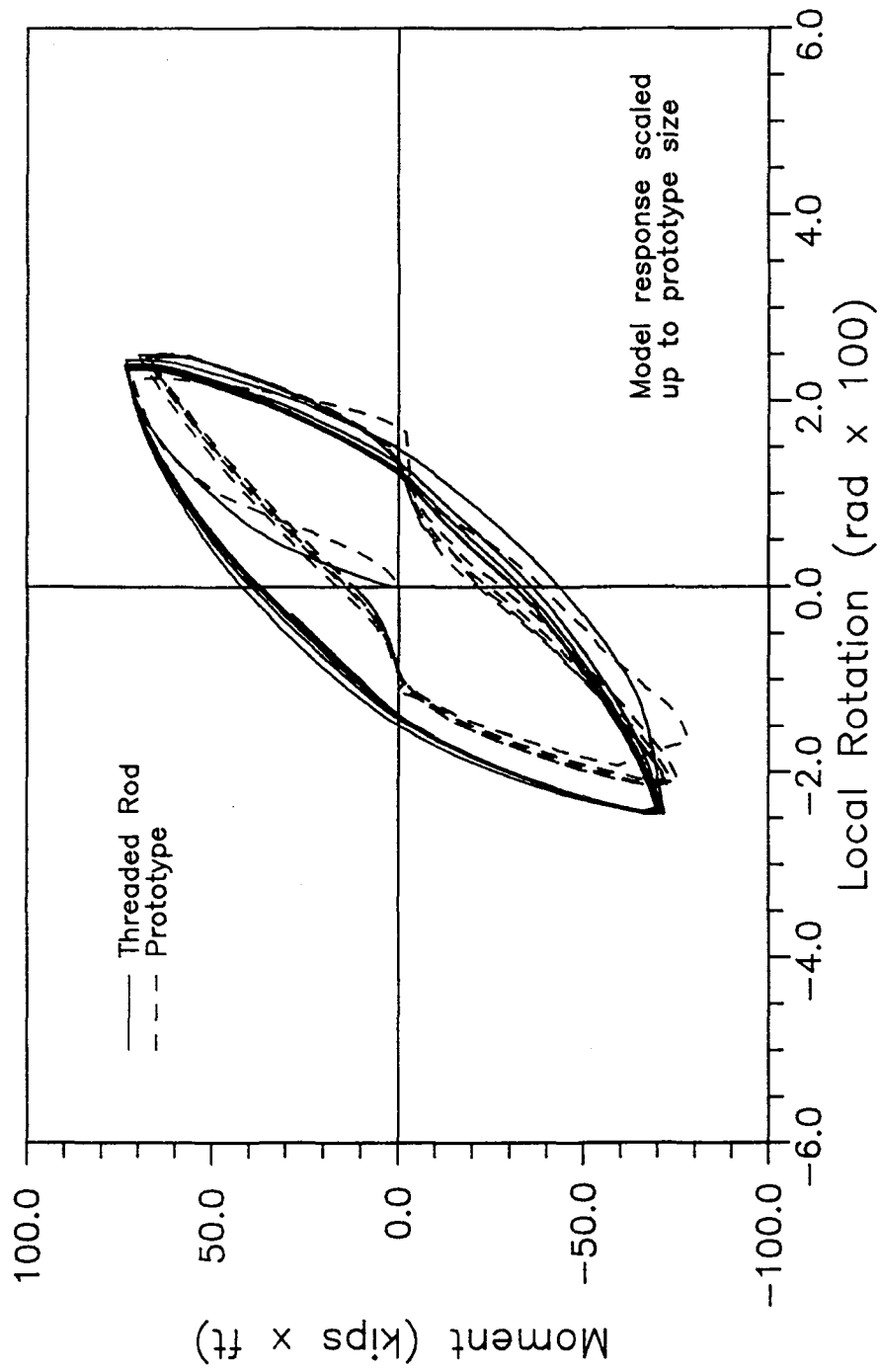
Figure 4.14.b.  Threaded Rod Versus Prototype Response at a Ductility Factor of 3.
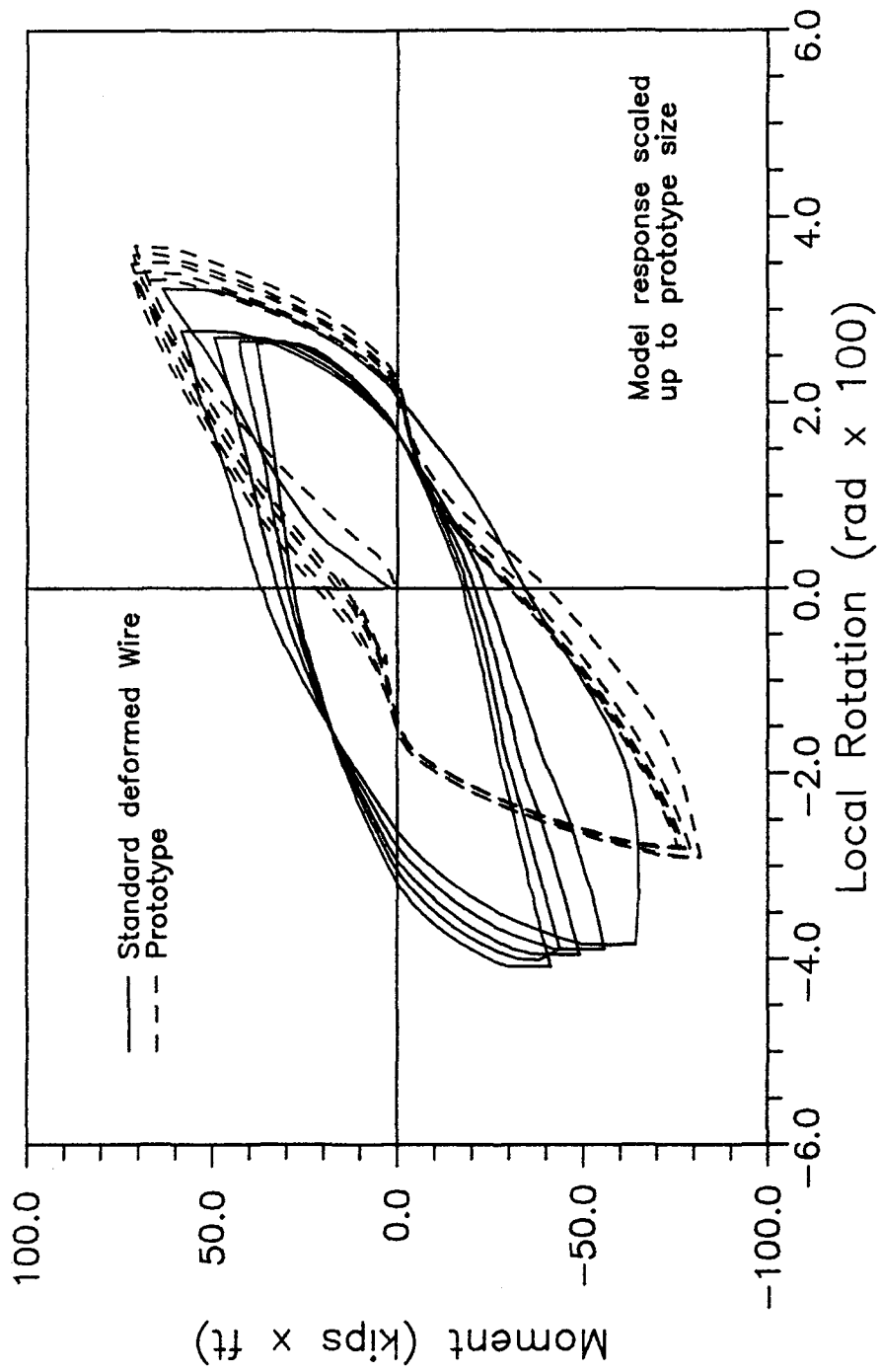
Figure 4.15.a. Standard Deformed Wire Versus Prototype
Response at a Ductility Factor of 4.
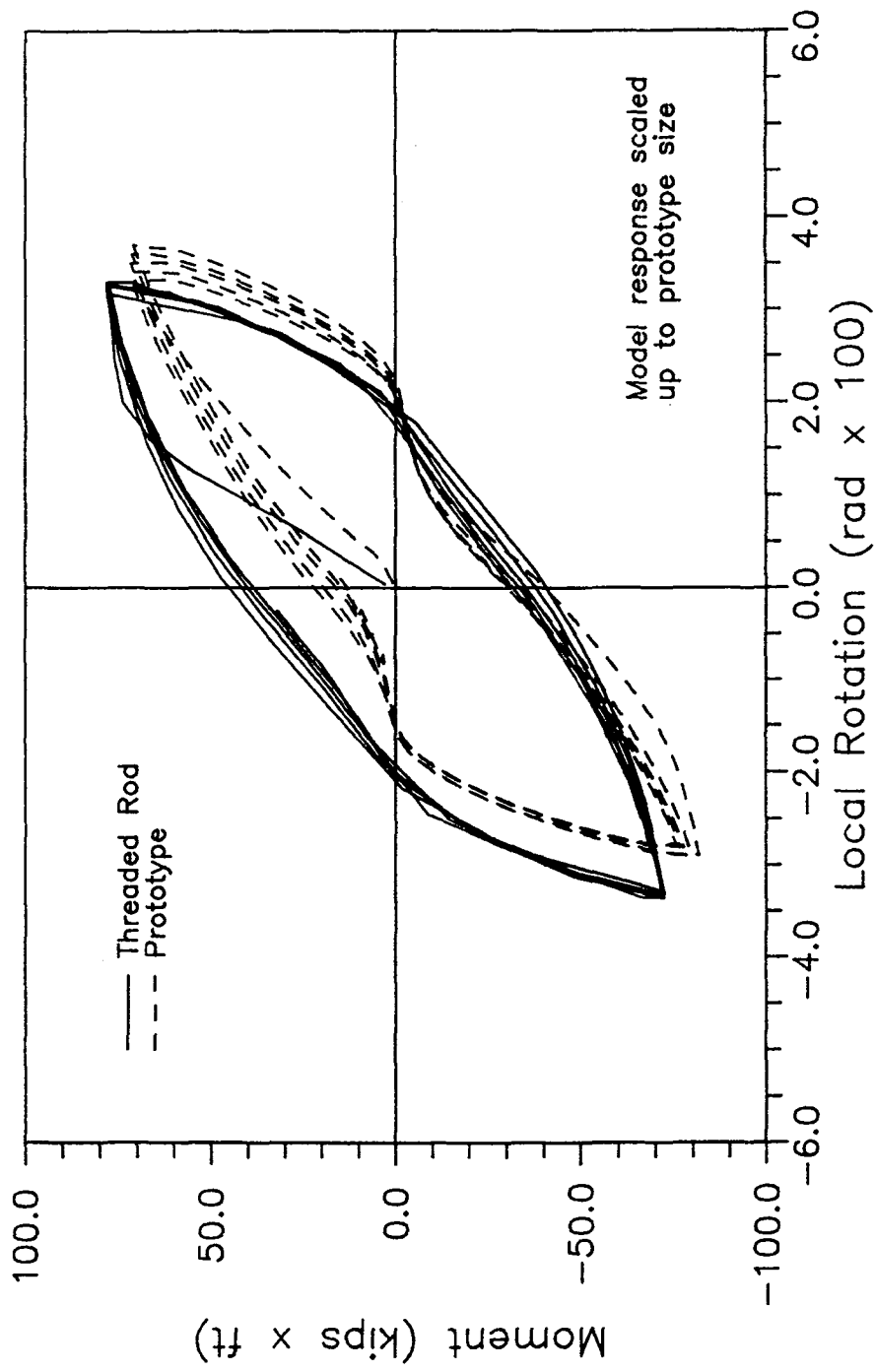
Figure 4.15.b. Threaded Rod Versus Prototype Response
at a Ductility Factor of 4.
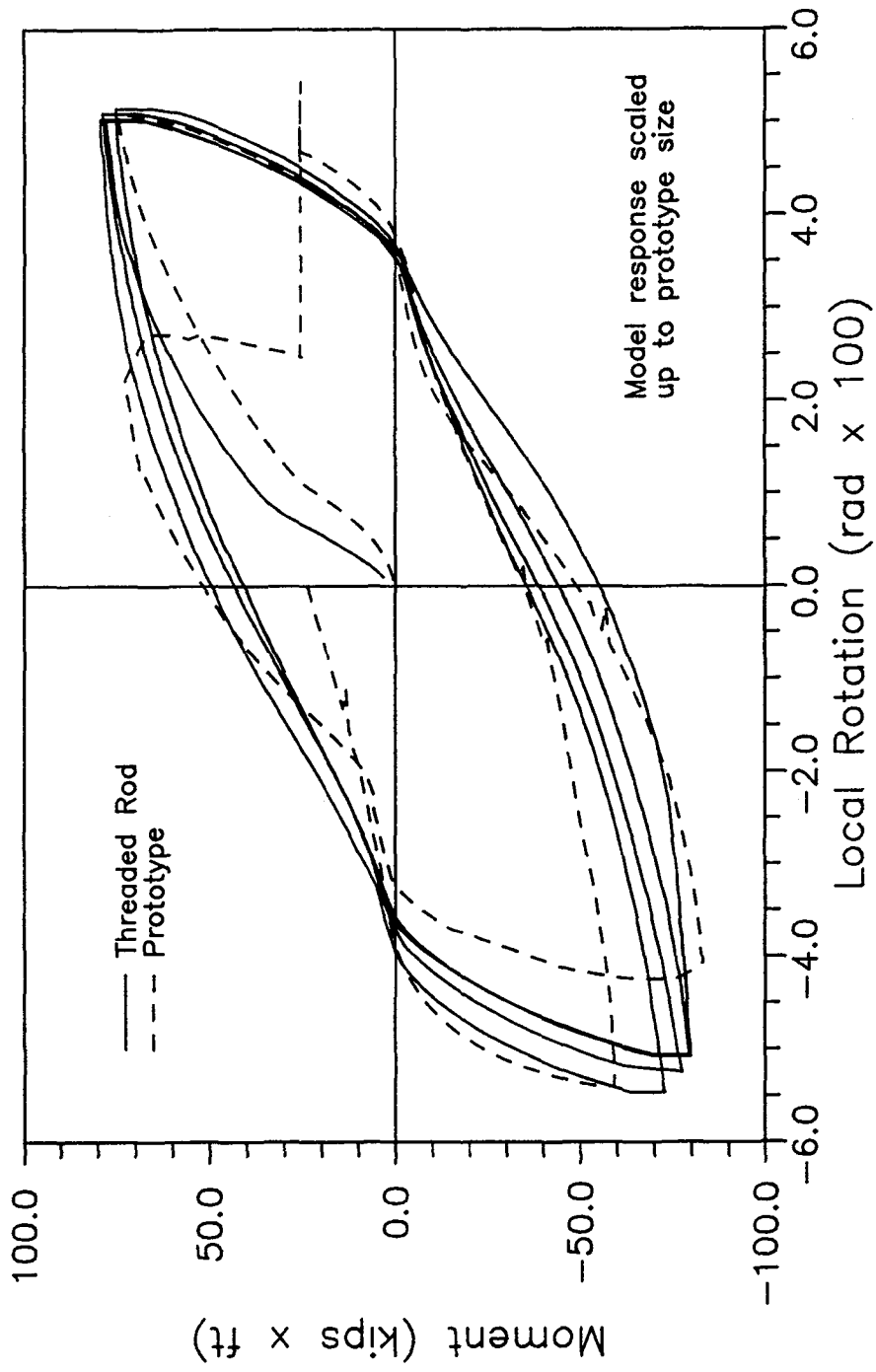
Figure 4.16. Threaded Rod Versus Prototype Response at a Ductility Factor of 6.

Due to the spalling of the prototype cover, the instruments providing the rotation readings were reattached after the first cycle, and a near zero reading was taken. After the second cycle, it was impossible to continue the test. This is shown in the jump in the prototype hysteresis loop shown in Figure 4.16). The threaded bars model also showed significant reduction of strength after the 5th cycle at ductility factor of 6.0 (Figure 4.16).

# CHAPTER 5
## SUMMARY AND CONCLUSIONS

The primary purpose of this research was to improve the materials used for the construction of small scale models of reinforced concrete structures subjected to severe cyclic loads such as those experienced in earthquakes. Attention was focused on the influence of model concrete mix design on compressive and tensile strengths and modulus of elasticity, on the optimal types of deformations to be used on model reinforcement, and on comparison of prototype behavior with small scale model behavior to determine which combination of materials provide the best modeling of cracking and hysteretic behavior.

A detailed study of influence of particle size and gradation on model concrete properties was conducted to best model prototype concrete strength (compression and tension) and stiffness.

Model reinforcement considered included plain wires, threaded rods, and model reinforcement with deformations scaled to match prototype reinforcement. All the reinforcing steels were heat treated to provide an accurate value of yield strength for each type of model reinforcement.

A prototype cantilever beam-type specimen was constructed and loaded with fully reversing flexural load to provide a basis of comparison of three 1/6 scale models of the same design and load history. The loading included a number of reversing loads with ductility factors of 0.5, 2, 3, 4, and 6. Test results from the prototype and model specimens were compared to evaluate the new modeling techniques.

On the basis of the results of this study, the following conclusions may be drawn:

1.  Prototype concrete stress-strain curve can be accurately modeled by careful selection of aggregate, aggregate grading, and water/cement ratio.

2.  The use of threaded bars as model reinforcement is the best available option since this type of reinforcing provides;
    -  Nearly perfect modeling at low deformation load cycles (up to ductility factor of 2.0).
    -  Correct ultimate strength even after severe cycling.

- Good duplication of cracking pattern and local behavior at different stages of loading.

- Models made with threaded bar reinforcement give results that are slightly unconservative because of the lack of sufficient pinching in the hysteresis curves. The energy absorbed by the threaded bars model is about 10% more than that of the prototype. "Flatter," customized threads should give better results.

# REFERENCES

1.  ACI Committee 444, "State-of-the-Art Report: Models of Reinforced Concrete Members," American Concrete Institute, Detroit, Michigan, 1977.

2.  ACI Ad Hoc Committee on Structural Models, "Models for Concrete Structures," ACI Special Publication No. 24, Detroit, Michigan, 1970.

3.  Sabnis, G. M., Harris, H. G., White, R. N., and Mirza, M. S., <u>Structural Modeling and Experimental Techniques</u>, Prentice-Hall Inc., Englewood Cliff, New Jersey, 1983.

4.  White, R. N., "Modeling Techniques for Reinforced Concrete Structures," Report No. 326, Dept. of Structural Engineering, Cornell University, 1976.

5.  Harris, H. G., Editor, "Dynamic Modeling of Concrete Structures," Publication SP-73, American Concrete Institute, Detroit, Michigan, 1982.

6.  Bertero, V. V., Aktan, A. E., Harris, H. G., and Chowdhury, A. A., "Mechanical Characteristics of Materials Used in a 1/5 Scale Model of a 7-Story Reinforced Concrete Test Structure," Report No. UCB/EERC-83/21 College of Engineering, University of California, Berkeley, California, 1983.

7.  Bedell, R. J., and Abrams, D. P., "Scale Relationships of Concrete Columns," Structural Research Series No. 8302, University of Colorado, Boulder, Colorado, 1983.

8.  Marayama, Y., and Noda, S., "Study on Small Scale Model Tests for Reinforced Concrete Structures - Small Scale Model Tests by Using 3mm Diameter Deformed Rebars," Report No. 40, Kajima Institute of Construction Technology, Tokyo, Japan, 1983.

9.  Darwin, D., "The Effect of Paste - Aggregate Bond Strength Upon the Behavior of Portland Cement Concrete Under Short-Term Load," M.S. Thesis, Cornell University, Ithaca, New York, 1968.

10. Noor, F. A., Wijayasri, S., "Modeling the Stress-Strain Relationship of Structural Concrete," Magazine of Concrete Research, Vol. 34, No. 116, March, 1983.

11. Harris, H. G., Sabnis, G. M., and White, R. N., "Small Scale Direct Models of Reinforced and Prestressed Concrete Structures," Report No. 376, Cornell University, September 1966.

# NATIONAL CENTER FOR EARTHQUAKE ENGINEERING RESEARCH
## LIST OF PUBLISHED TECHNICAL REPORTS

The National Center for Earthquake Engineering Research (NCEER) publishes technical reports on a variety of subjects related to earthquake engineering written by authors funded through NCEER. These reports are available from both NCEER's Publications Department and the National Technical Information Service (NTIS). Requests for reports should be directed to the Publications Department, National Center for Earthquake Engineering Research, State University of New York at Buffalo, Red Jacket Quadrangle, Buffalo, New York 14261. Reports can also be requested through NTIS, 5285 Port Royal Road, Springfield, Virginia 22161. NTIS accession numbers are shown in parenthesis, if available.

NCEER-87-0001 "First-Year Program in Research, Education and Technology Transfer," 3/5/87, (PB88-134275/AS).

NCEER-87-0002 "Experimental Evaluation of Instantaneous Optimal Algorithms for Structural Control," by R.C. Lin, T.T. Soong and A.M. Reinhorn, 4/20/87, (PB88-134341/AS).

NCEER-87-0003 "Experimentation Using the Earthquake Simulation Facilities at University at Buffalo," by A.M. Reinhorn and R.L. Ketter, to be published.

NCEER-87-0004 "The System Characteristics and Performance of a Shaking Table," by J.S. Hwang, K.C. Chang and G.C. Lee, 6/1/87, (PB88-134259/AS).

NCEER-87-0005 "A Finite Element Formulation for Nonlinear Viscoplastic Material Using a Q Model," by O. Gyebi and G. Dasgupta, 11/2/87, (PB88-213764/AS).

NCEER-87-0006 "Symbolic Manipulation Program (SMP) - Algebraic Codes for Two and Three Dimensional Finite Element Formulations," by X. Lee and G. Dasgupta, 11/9/87, (PB88-219522/AS).

NCEER-87-0007 "Instantaneous Optimal Control Laws for Tall Buildings Under Seismic Excitations," by J.N. Yang, A. Akbarpour and P. Ghaemmaghami, 6/10/87, (PB88-134333/AS).

NCEER-87-0008 "IDARC: Inelastic Damage Analysis of Reinforced Concrete Frame - Shear-Wall Structures," by Y.J. Park, A.M. Reinhorn and S.K. Kunnath, 7/20/87, (PB88-134325/AS).

NCEER-87-0009 "Liquefaction Potential for New York State: A Preliminary Report on Sites in Manhattan and Buffalo," by M. Budhu, V. Vijayakumar, R.F. Giese and L. Baumgras, 8/31/87, (PB88-163704/AS). This report is available only through NTIS (see address given above).

NCEER-87-0010 "Vertical and Torsional Vibration of Foundations in Inhomogeneous Media," by A.S. Veletsos and K.W. Dotson, 6/1/87, (PB88-134291/AS).

NCEER-87-0011 "Seismic Probabilistic Risk Assessment and Seismic Margins Studies for Nuclear Power Plants," by Howard H.M. Hwang, 6/15/87, (PB88-134267/AS). This report is available only through NTIS (see address given above).

NCEER-87-0012 "Parametric Studies of Frequency Response of Secondary Systems Under Ground-Acceleration Excitations," by Y. Yong and Y.K. Lin, 6/10/87, (PB88-134309/AS).

NCEER-87-0013 "Frequency Response of Secondary Systems Under Seismic Excitation," by J.A. HoLung, J. Cai and Y.K. Lin, 7/31/87, (PB88-134317/AS).

NCEER-87-0014 "Modelling Earthquake Ground Motions in Seismically Active Regions Using Parametric Time Series Methods," by G.W. Ellis and A.S. Cakmak, 8/25/87, (PB88-134283/AS).

NCEER-87-0015 "Detection and Assessment of Seismic Structural Damage," by E. DiPasquale and A.S. Cakmak, 8/25/87, (PB88-163712/AS).

NCEER-87-0016 "Pipeline Experiment at Parkfield, California," by J. Isenberg and E. Richardson, 9/15/87, (PB88-163720/AS).

NCEER-87-0017        "Digital Simulation of Seismic Ground Motion," by M. Shinozuka, G. Deodatis and T. Harada, 8/31/87, (PB88-155197/AS). This report is available only through NTIS (see address given above).

NCEER-87-0018        "Practical Considerations for Structural Control: System Uncertainty, System Time Delay and Truncation of Small Control Forces," J.N. Yang and A. Akbarpour, 8/10/87, (PB88-163738/AS).

NCEER-87-0019        "Modal Analysis of Nonclassically Damped Structural Systems Using Canonical Transformation," by J.N. Yang, S. Sarkani and F.X. Long, 9/27/87, (PB88-187851/AS).

NCEER-87-0020        "A Nonstationary Solution in Random Vibration Theory," by J.R. Red-Horse and P.D. Spanos, 11/3/87, (PB88-163746/AS).

NCEER-87-0021        "Horizontal Impedances for Radially Inhomogeneous Viscoelastic Soil Layers," by A.S. Veletsos and K.W. Dotson, 10/15/87, (PB88-150859/AS).

NCEER-87-0022        "Seismic Damage Assessment of Reinforced Concrete Members," by Y.S. Chung, C. Meyer and M. Shinozuka, 10/9/87, (PB88-150867/AS). This report is available only through NTIS (see address given above).

NCEER-87-0023        "Active Structural Control in Civil Engineering," by T.T. Soong, 11/11/87, (PB88-187778/AS).

NCEER-87-0024        Vertical and Torsional Impedances for Radially Inhomogeneous Viscoelastic Soil Layers," by K.W. Dotson and A.S. Veletsos, 12/87, (PB88-187786/AS).

NCEER-87-0025        "Proceedings from the Symposium on Seismic Hazards, Ground Motions, Soil-Liquefaction and Engineering Practice in Eastern North America," October 20-22, 1987, edited by K.H. Jacob, 12/87, (PB88-188115/AS).

NCEER-87-0026        "Report on the Whittier-Narrows, California, Earthquake of October 1, 1987," by J. Pantelic and A. Reinhorn, 11/87, (PB88-187752/AS). This report is available only through NTIS (see address given above).

NCEER-87-0027        "Design of a Modular Program for Transient Nonlinear Analysis of Large 3-D Building Structures," by S. Srivastav and J.F. Abel, 12/30/87, (PB88-187950/AS).

NCEER-87-0028        "Second-Year Program in Research, Education and Technology Transfer," 3/8/88, (PB88-219480/AS).


NCEER-88-0001        "Workshop on Seismic Computer Analysis and Design of Buildings With Interactive Graphics," by W. McGuire, J.F. Abel and C.H. Conley, 1/18/88, (PB88-187760/AS).

NCEER-88-0002        "Optimal Control of Nonlinear Flexible Structures," by J.N. Yang, F.X. Long and D. Wong, 1/22/88, (PB88-213772/AS).

NCEER-88-0003        "Substructuring Techniques in the Time Domain for Primary-Secondary Structural Systems," by G.D. Manolis and G. Juhn, 2/10/88, (PB88-213780/AS).

NCEER-88-0004        "Iterative Seismic Analysis of Primary-Secondary Systems," by A. Singhal, L.D. Lutes and P.D. Spanos, 2/23/88, (PB88-213798/AS).

NCEER-88-0005        "Stochastic Finite Element Expansion for Random Media," by P.D. Spanos and R. Ghanem, 3/14/88, (PB88-213806/AS).

NCEER-88-0006        "Combining Structural Optimization and Structural Control," by F.Y. Cheng and C.P. Pantelides, 1/10/88, (PB88-213814/AS).

NCEER-88-0007        "Seismic Performance Assessment of Code-Designed Structures," by H.H-M. Hwang, J-W. Jaw and H-J. Shau, 3/20/88, (PB88-219423/AS).

NCEER-88-0008      "Reliability Analysis of Code-Designed Structures Under Natural Hazards," by H.H-M. Hwang, H. Ushiba and M. Shinozuka, 2/29/88, (PB88-229471/AS).

NCEER-88-0009      "Seismic Fragility Analysis of Shear Wall Structures," by J-W Jaw and H.H-M. Hwang, 4/30/88.

NCEER-88-0010      "Base Isolation of a Multi-Story Building Under a Harmonic Ground Motion - A Comparison of Performances of Various Systems," by F-G Fan, G. Ahmadi and I.G. Tadjbakhsh, 5/18/88.

NCEER-88-0011      "Seismic Floor Response Spectra for a Combined System by Green's Functions," by F.M. Lavelle, L.A. Bergman and P.D. Spanos, 5/1/88.

NCEER-88-0012      "A New Solution Technique for Randomly Excited Hysteretic Structures," by G.Q. Cai and Y.K. Lin, 5/16/88.

NCEER-88-0013      "A Study of Radiation Damping and Soil-Structure Interaction Effects in the Centrifuge," by K. Weissman, supervised by J.H. Prevost, 5/24/88.

NCEER-88-0014      "Parameter Identification and Implementation of a Kinematic Plasticity Model for Frictional Soils," by J.H. Prevost and D.V. Griffiths, to be published.

NCEER-88-0015      "Two- and Three- Dimensional Dynamic Finite Element Analyses of the Long Valley Dam," by D.V. Griffiths and J.H. Prevost, 6/17/88.

NCEER-88-0016      "Damage Assessment of Reinforced Concrete Structures in Eastern United States," by A.M. Reinhorn, M.J. Seidel, S.K. Kunnath and Y.J. Park, 6/15/88.

NCEER-88-0017      "Dynamic Compliance of Vertically Loaded Strip Foundations in Multilayered Viscoelastic Soils," by S. Ahmad and A.S.M. Israil, 6/17/88.

NCEER-88-0018      "An Experimental Study of Seismic Structural Response With Added Viscoelastic Dampers," by R.C. Lin, Z. Liang, T.T. Soong and R.H. Zhang, 6/30/88.

NCEER-88-0019      "Experimental Investigation of Primary - Secondary System Interaction," by G.D. Manolis, G. Juhn and A.M. Reinhorn, 5/27/88.

NCEER-88-0020      "A Response Spectrum Approach For Analysis of Nonclassically Damped Structures," by J.N. Yang, S. Sarkani and F.X. Long, 4/22/88.

NCEER-88-0021      "Seismic Interaction of Structures and Soils: Stochastic Approach," by A.S. Veletsos and A.M. Prasad, 7/21/88.

NCEER-88-0022      "Identification of the Serviceability Limit State and Detection of Seismic Structural Damage," by E. DiPasquale and A.S. Cakmak, 6/15/88.

NCEER-88-0023      "Multi-Hazard Risk Analysis: Case of a Simple Offshore Structure," by B.K. Bhartia and E.H. Vanmarcke, 7/21/88.

NCEER-88-0024      "Automated Seismic Design of Reinforced Concrete Buildings," by Y.S. Chung, C. Meyer and M. Shinozuka, 7/5/88.

NCEER-88-0025      "Experimental Study of Active Control of MDOF Structures Under Seismic Excitations," by L.L. Chung, R.C. Lin, T.T. Soong and A.M. Reinhorn, 7/10/88, (PB89-122600/AS).

NCEER-88-0026      "Earthquake Simulation Tests of a Low-Rise Metal Structure," by J.S. Hwang, K.C. Chang, G.C. Lee and R.L. Ketter, 8/1/88.

NCEER-88-0027      "Systems Study of Urban Response and Reconstruction Due to Catastrophic Earthquakes," by F. Kozin and H.K. Zhou, 9/22/88, to be published.

NCEER-88-0028    "Seismic Fragility Analysis of Plane Frame Structures," by H.H-M. Hwang and Y.K. Low, 7/31/88, (PB89-131445/AS).

NCEER-88-0029    "Response Analysis of Stochastic Structures," by A. Kardara, C. Bucher and M. Shinozuka, 9/22/88.

NCEER-88-0030    "Nonnormal Accelerations Due to Yielding in a Primary Structure," by D.C.K. Chen and L.D. Lutes, 9/19/88.

NCEER-88-0031    "Design Approaches for Soil-Structure Interaction," by A.S. Veletsos, A.M. Prasad and Y. Tang, 12/30/88.

NCEER-88-0032    "A Re-evaluation of Design Spectra for Seismic Damage Control," by C.J. Turkstra and A.G. Tallin, 11/7/88, (PB89-145221/AS).

NCEER-88-0033    "The Behavior and Design of Noncontact Lap Splices Subjected to Repeated Inelastic Tensile Loading," by V.E. Sagan, P. Gergely and R.N. White, 12/8/88.

NCEER-88-0034    "Seismic Response of Pile Foundations," by S.M. Mamoon, P.K. Banerjee and S. Ahmad, 11/1/88, (PB89-145239/AS).

NCEER-88-0035    "Modeling of R/C Building Structures With Flexible Floor Diaphragms (IDARC2)," by A.M. Reinhorn, S.K. Kunnath and N. Panahshahi, 9/7/88.

NCEER-88-0036    "Solution of the Dam-Reservoir Interaction Problem Using a Combination of FEM, BEM with Particular Integrals, Modal Analysis, and Substructuring," by C-S. Tsai, G.C. Lee and R.L. Ketter, 12/31/88, to be published.

NCEER-88-0037    "Optimal Placement of Actuators for Structural Control," by F.Y. Cheng and C.P. Pantelides, 8/15/88.

NCEER-88-0038    "Teflon Bearings in Aseismic Base Isolation: Experimental Studies and Mathematical Modeling," by A. Mokha, M.C. Constantinou and A.M. Reinhorn, 12/5/88.

NCEER-88-0039    "Seismic Behavior of Flat Slab High-Rise Buildings in the New York City Area," by P. Weidlinger and M. Ettouney, 10/15/88, to be published.

NCEER-88-0040    "Evaluation of the Earthquake Resistance of Existing Buildings in New York City," by P. Weidlinger and M. Ettouney, 10/15/88, to be published.

NCEER-88-0041    "Small-Scale Modeling Techniques for Reinforced Concrete Structures Subjected to Seismic Loads," by W. Kim, A. El-Attar and R.N. White, 11/22/88.